Structure of the essential inner membrane lipopolysaccharide–PbgA complex

https://doi.org/10.1038/s41586-020-2597-x

Received: 22 March 2018

Accepted: 10 July 2020

Published online: 12 August 2020

Thomas Clairfeuille[1,13], Kerry R. Buchholz[2,13], Qingling Li[3], Erik Verschueren[3], Peter Liu[3], Dewakar Sangaraju[4], Summer Park[5], Cameron L. Noland[1], Kelly M. Storek[2], Nicholas N. Nickerson[2], Lynn Martin[6], Trisha Dela Vega[6], Anh Miu[7], Janina Reeder[8], Maria Ruiz-Gonzalez[9], Danielle Swem[2], Guanghui Han[3], Daniel P. DePonte[10], Mark S. Hunter[10], Cornelius Gati[11,12], Sheerin Shahidi-Latham[4], Min Xu[5], Nicholas Skelton[9], Benjamin D. Sellers[9], Elizabeth Skippington[8], Wendy Sandoval[3], Emily J. Hanan[9]✉, Jian Payandeh[1,2]✉ & Steven T. Rutherford[2]✉

Lipopolysaccharide (LPS) resides in the outer membrane of Gram-negative bacteria where it is responsible for barrier function[1,2]. LPS can cause death as a result of septic shock, and its lipid A core is the target of polymyxin antibiotics[3,4]. Despite the clinical importance of polymyxins and the emergence of multidrug resistant strains[5], our understanding of the bacterial factors that regulate LPS biogenesis is incomplete. Here we characterize the inner membrane protein PbgA and report that its depletion attenuates the virulence of *Escherichia coli* by reducing levels of LPS and outer membrane integrity. In contrast to previous claims that PbgA functions as a cardiolipin transporter[6–9], our structural analyses and physiological studies identify a lipid A-binding motif along the periplasmic leaflet of the inner membrane. Synthetic PbgA-derived peptides selectively bind to LPS in vitro and inhibit the growth of diverse Gram-negative bacteria, including polymyxin-resistant strains. Proteomic, genetic and pharmacological experiments uncover a model in which direct periplasmic sensing of LPS by PbgA coordinates the biosynthesis of lipid A by regulating the stability of LpxC, a key cytoplasmic biosynthetic enzyme[10–12]. In summary, we find that PbgA has an unexpected but essential role in the regulation of LPS biogenesis, presents a new structural basis for the selective recognition of lipids, and provides opportunities for future antibiotic discovery.

In *E. coli*, the outer membrane is an essential structure where LPS resides within the outer leaflet to impart barrier function and immune modulation[1]. Cell division requires the synthesis and transport of millions of new LPS molecules[1,2], which are composed of a lipid A membrane-anchor, core oligosaccharide, and O-antigen. LpxC performs the committed step of lipid A biosynthesis[13], and after the addition of core oligosaccharides, MsbA flips LPS into the periplasmic leaflet of the inner membrane[1,2]. The $LptB_2FG$ complex shuttles mature LPS across the periplasm to LptDE, which promotes LPS insertion into the outer membrane[1,2]. The outer membrane contains phospholipids on the inner leaflet and imbalance of the LPS-to-phospholipid ratio compromises outer membrane function and cell viability[2]. Information about LPS physiology within the inner membrane remains limited, and the mechanisms that coordinate its synthesis and transport to the outer membrane are poorly defined.

PbgA is an enigmatic inner membrane protein proposed to assemble as a homotetrameric complex that shuttles cardiolipin across the periplasm to the outer membrane[6–9]. However, recent structural studies did not conclusively establish direct evidence of cardiolipin binding and transport[7,8,14]. We investigated PbgA because it is required for the pathogenesis of *Salmonella*[6], conserved in *Enterobacteriaceae*, and has an unclear role in maintaining the outer membrane[10,11,15–18]. Our PbgA crystal structure revealed an unanticipated lipid A-binding motif that has uncovered a new paradigm in bacterial physiology in which PbgA directly perceives LPS within the inner membrane to control the cellular balance of LPS biosynthesis by regulating levels of LpxC. We also report the characterization of lipid A-targeting synthetic peptides based on PbgA that can inhibit the growth of diverse Gram-negative pathogens.

PbgA is essential for outer membrane integrity

Our uropathogenic *E. coli* (UPEC) *pbgA* deletion (Δ*pbgA*) strain contained a suppressor mutation, which suggests *pbgA* essentiality[6,18]. This strain was cleared from mice, serum sensitive, and sensitized to large antibiotics that normally cannot penetrate the outer membrane

[1]Structural Biology, Genentech Inc., South San Francisco, CA, USA. [2]Infectious Diseases, Genentech Inc., South San Francisco, CA, USA. [3]Microchemistry, Proteomics & Lipidomics, Genentech Inc., South San Francisco, CA, USA. [4]Drug Metabolism & Pharmacokinetics, Genentech Inc., South San Francisco, CA, USA. [5]Translational Immunology, Genentech Inc., South San Francisco, CA, USA. [6]BioMolecular Resources, Genentech Inc., South San Francisco, CA, USA. [7]Biochemical & Cellular Pharmacology, Genentech Inc., South San Francisco, CA, USA. [8]Bioinformatics & Computational Biology, Genentech Inc., South San Francisco, CA, USA. [9]Discovery Chemistry Departments, Genentech Inc., South San Francisco, CA, USA. [10]Linac Coherent Light Source, SLAC National Accelerator Laboratory, Menlo Park, CA, USA. [11]Bioscience Division, SLAC National Accelerator Laboratory, Menlo Park, CA, USA. [12]Stanford University, Department of Structural Biology, Stanford, CA, USA. [13]These authors contributed equally: Thomas Clairfeuille, Kerry R. Buchholz. ✉e-mail: hanan.emily@gene.com; payandeh.jian@gene.com; rutherford.steven@gene.com

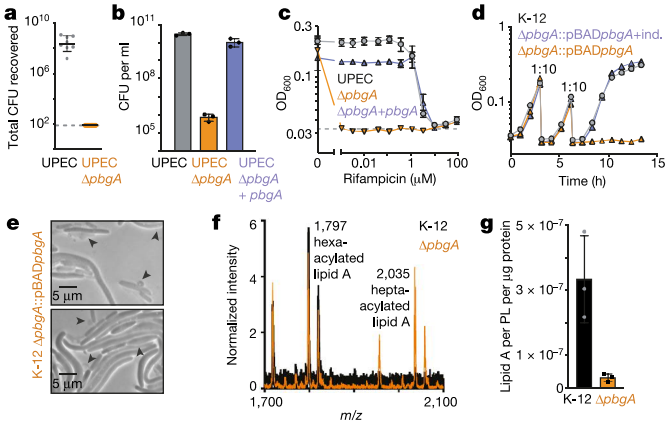

Fig. 1 | PbgA is essential for outer membrane integrity. a, Colony-forming units (CFUs) recovered from the thigh muscle of neutropenic CD1 mice ($n = 8$ per group) 24 h after intramuscular injection. **b**, Strain sensitivity to 50% human serum. **c**, Rifampicin sensitivity of UPEC and UPEC Δ*pbgA* strains diluted into fresh medium containing rifampicin. OD_{600} values were determined at 6 h. **d**, *E. coli* K-12 Δ*pbgA*::pBAD*pbgA* cultures diluted in fresh medium with or without inducer (0.02% arabinose). **e**, *E. coli* K-12 Δ*pbgA*::pBAD*pbgA* grown without arabinose. Images were taken at 4 h and are representative of $n = 3$ experiments. Scale bars, 5 μm. **f**, MALDI–TOF analysis of lipid A extracts from outer membrane vesicles, representative of $n = 3$ experiments. **g**, Quantification of lipid A and phospholipid (PL) by MALDI–TOF analysis of outer membrane vesicles. Data in **a**–**d**, **g** are mean ± s.d. from $n = 3$ independent cultures; line in **a** indicates lower boundary of detection.

(Fig. 1a–c, Extended Data Fig. 1a, Supplementary Table 1). Serum and rifampicin sensitivities were complemented by reintroducing *pbgA* on a plasmid (Fig. 1b, c). In the absence of a suppressor mutation, depletion of PbgA in *E. coli* K-12 resulted in inhibition of growth, rifampicin sensitivity, cells with increased diameter, loss of shape, and membrane bursting (Fig. 1d, e, Extended Data Fig. 1b). Indicating disturbed lipid homeostasis, outer membrane vesicles showed increased hepta-acylated lipid A species and a decrease in the total lipid A:phospholipid ratio relative to wild-type strains[15,19] (Fig. 1f, g). A strain devoid of cardiolipin (Δ*clsABC*) was not sensitized to rifampicin[18,20] (Extended Data Fig. 1c–e). These results establish an essential role for PbgA in pathogenesis, growth and maintaining outer membrane barrier function in *E. coli* in the absence of cardiolipin synthesis.

PbgA is a pseudo-hydrolase

Purified PbgA was monomeric in mild detergent and stabilized by anionic phospholipids, including phospholipid species not naturally abundant in *E. coli* (Extended Data Fig. 2a, b). PbgA crystallized in lipidic cubic phases and the addition of phosphatidylethanolamine allowed high-resolution structure determination (approximately 2 Å), revealing numerous extra densities around the transmembrane domain (TMD) (Extended Data Fig. 2c, d, Supplementary Table 2). PbgA contains five N-terminal transmembrane helices upon which the C-terminal periplasmic domain sits (Fig. 2a). The interfacial domain (IFD) is a compacted three-helix bundle that connects the TMD and periplasmic domain, where substantial interdomain contacts (approximately 2,550 $Å^2$) suggest the TMD, IFD and periplasmic domain are tightly fused together (Fig. 2a, b, Extended Data Fig. 2e). A distinct crystal form, molecular dynamics studies, and comparison to a recent structure[7] revealed no substantive conformational changes (Extended Data Fig. 3a, b, Supplementary Table 2), indicating that the periplasmic domain remains anchored onto the TMD and protrudes only 60 Å above the inner membrane (Fig. 2a, b). These findings oppose the cardiolipin-transporter model that suggests that the periplasmic domain shuttles across the periplasm[6], which typically measures around 200 Å[21]. Moreover, the IFD is not a simple linker as previously proposed[6], the cardiolipin-binding site hypothesized within the periplasmic domain[8] is distant from the inner membrane and probably cannot permit phospholipid access (Extended Data Fig. 3c), and PbgA is not related to any known transporter (Supplementary Table 3).

PbgA is structurally related to a superfamily of enzymes that modify the cell envelopes of Gram-negative and Gram-positive bacteria (Supplementary Table 3). The periplasmic domain is similar to LtaS, a Mn^{2+}-dependent enzyme that synthesizes an abundant surface polymer in *Staphylococcus aureus*, which lack an outer membrane[22] (Extended Data Fig. 3d). The full-length PbgA structure is most similar to EptA, an inner membrane-anchored, Zn^{2+}-dependent enzyme that transfers a phosphoethanolamine moiety onto lipid A to impart resistance to polymyxin (PMX)[5,23]. Although isolated periplasmic domains and TMDs superimpose well, the compacted α-helical IFD of PbgA exists as an extended linker in EptA, so overall architectures are highly divergent (Extended Data Fig. 3e). Notably, PbgA does not conserve the side chains required to coordinate Zn^{2+} and mutations within its vestigial active site do not affect outer membrane integrity (Fig. 2c, d). Thus, the periplasmic domain appears to be a pseudo-hydrolase, and PbgA has evolved to support an unknown essential function in *E. coli*.

An unanticipated lipid A-binding motif

Strong extra density is observed along the periplasmic membrane leaflet cradled against the IFD of PbgA, but attempts to model or detect cardiolipin failed (Extended Data Figs. 2c, 4a, Supplementary Table 4). Two assays identified the presence of lipid A, and modelling of lipid A rationalized the distinctive bilobal electron density (Extended Data Figs. 2c, 4a–c). Thus, a co-purifying LPS molecule remains bound to PbgA, where the IFD is entirely responsible for coordination using a highly conserved periplasmic lipid A-binding motif (Figs. 2a, b, 3a–d).

PbgA recognizes a minimal feature of lipid A, a single phospho-GlcNAc unit, using eight consecutive residues that precede and form part of the α7-helix, 210-YPMTARRF-217 (Fig. 3b). Specifically, Phe217 anchors the α7-helix within the membrane, and its backbone bonds through water to the *R*-3-hydroxymyristoyl and 1-phospho-GlcNAc of lipid A (Fig. 3b, d). Amides of Arg216 and Arg215 complex with the 1-phospho-GlcNAc, which is further stabilized by the α7-helical dipole (Fig. 3b, d). Notably, the Arg216 side chain is not conserved in all PbgA homologues, and the Arg215 side chain interacts structurally with a conserved acidic residue in the TMD (Extended Data Figs. 2f, 5). Ala214 links to the 210-YPMT-213 segment, allowing the Thr213 backbone to engage the 3-linked *R*-3-hydroxymyristoyl group, and the Thr213 hydroxyl to interact with the 1-hydroxyl and 1-phospho-GlcNAc positions (Fig. 3b). Met212 wedges between the 2- and 3-linked *R*-3-hydroxymyristoyl groups to form hydrophobic contacts (Fig. 3b, d). Pro211 and Tyr210 backbones bond to the 3-linked *R*-3-hydroxymyristoyl substituent, where Pro211 interacts through water (Fig. 3b). Overall, PbgA engages the distinctive chemistry of lipid A using a dense 14-point interaction network primarily through 10 backbone- and water-mediated interactions.

LPS–PbgA interface affects the outer membrane

We introduced point mutations into the PbgA lipid A-binding motif and evaluated outer membrane integrity (Fig. 3c, Extended Data Fig. 6). Charged variants of Met212 imparted sensitivity to rifampicin, in contrast to alanine mutation, which suggests that offending lipid A binding compromised the outer membrane (Fig. 3b–d). Mutation of Thr213 to valine (T213V) did not notably affect rifampicin sensitivity, whereas mutation to aspartic acid (T213D) intended to disrupt the interaction with the 1-phospho-GlcNAc produced extreme sensitization (Fig. 3b, c). Mutation of Arg216 to alanine had no effect, but acidic mutations intended to repulse the 1-phospho-GlcNAc group resulted in rifampicin sensitivities (Fig. 3b, c). The M212A/T213V/R216A triple

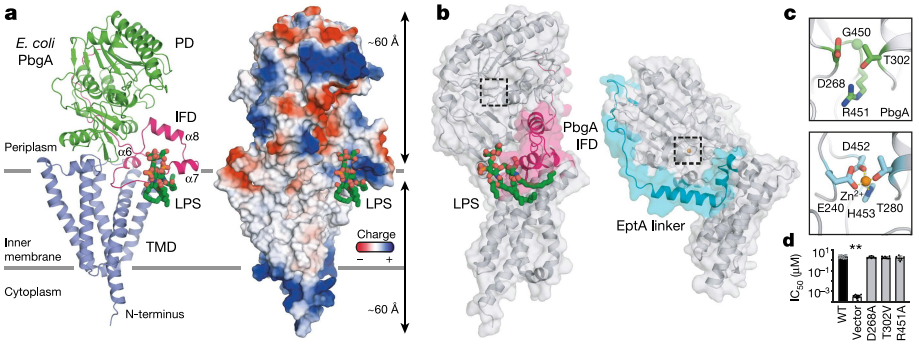

Fig. 2 | PbgA structural features. a, PbgA crystal structure in cartoon and electrostatic representation. TMD, IFD and periplasmic domain (PD) are in blue, pink and green, respectively, with LPS as green sticks. **b**, TMD-based alignment with the PbgA–IFD and EptA linker (PDB code 5FGN) in pink and cyan, respectively. Note that the EptA periplasmic domain is oriented approximately 180° relative to PbgA. **c**, Pseudo-hydrolase active site of PbgA (green) and catalytic site in EptA (cyan). **d**, Rifampicin sensitivity of UPEC Δ*pbgA* strains with plasmids expressing wild-type PbgA or mutants. Data are mean ± s.d. from $n = 6$ or more independent experiments per strain. $^{**}P < 0.001$, Bonferroni corrected unpaired two-tailed *t*-test.

mutant produced only a modest phenotype, highlighting the prominent multipoint backbone-mediated coordination scheme observed in PbgA (Fig. 3b–d). Thus, only mutations expected to disrupt lipid A binding along the periplasmic leaflet profoundly affected the outer membrane barrier, which suggests that the LPS–PbgA interface is an essential mediator of outer membrane homeostasis in *E. coli*.

PbgA-derived peptides bind LPS and kill *E. coli*

We postulated that a peptide derived solely from the IFD sequence might bind to LPS in vitro. A synthetic, linear peptide encompassing the lipid A-binding (LAB) motif from PbgA bound to LPS selectively (wild-type LAB (LAB_{WT}); dissociation constant (K_d) of approximately 75 μM) over all major *E. coli* phospholipids, whereas peptides expected to destabilize key lipid A-binding determinants ($LAB_{\Delta\alpha7}$ and LAB_{T213D}) showed no binding (Fig. 3e, Extended Data Fig. 7). We predicted that the H221W and D225R mutations might promote membrane partitioning and this LAB_{WT+} peptide (209-SYPMTARRFLEKWGLLR-225) had improved affinity for LPS (K_d value of approximately 55 μM) while maintaining selectivity over phospholipids (Fig. 3e).

Because PMX antibiotics kill Gram-negative bacteria by targeting lipid A[4,5], we tested the LAB peptides for antibacterial activity. The LAB_{WT} peptide had no effect on *E. coli* growth, potentially owing to its large molecular mass of greater than 2 kDa. For the LAB_{WT+} peptide, we measured minimal inhibitory concentrations (MICs) of 25–400 μM in chemically or genetically permeabilized cells (Supplementary Tables 5, 6). $LAB_{\Delta\alpha7}$ and LAB_{T213D} peptides, which were unable to bind LPS, showed no effect on cell growth under matched conditions (Supplementary Table 5). Alanine-scanning and truncation studies ultimately produced a synthetic peptide ($LAB_{v2.0}$) with an MIC of 200 μM against intact, wild-type *E. coli* K-12 (Supplementary Tables 5, 7, 8).

Optimized LAB achieves broad-spectrum activity

Starting from $LAB_{v2.0}$, structure-guided design suggested that T213Dap ((*S*)-2,3-diaminopropionic acid) should introduce a salt-bridge to the 1-phospho-GlcNAc, and A214F mutation might improve membrane partitioning and hydrophobic interactions with LPS (Fig. 3b, d). The resulting $LAB_{v2.1}$ peptide had an MIC of 25 μM against *E. coli* K-12 (Table 1). Inspection of our LPS–PbgA structure and associated data led to three predictions about $LAB_{v2.1}$ peptide activity (Fig. 3, Extended Data Fig. 4c). First, consistent with conservation of lipid A across Gram-negative bacteria[1], MICs of 12.5–200 μM were obtained against the clinically relevant pathogens *Enterobacter cloacae*,

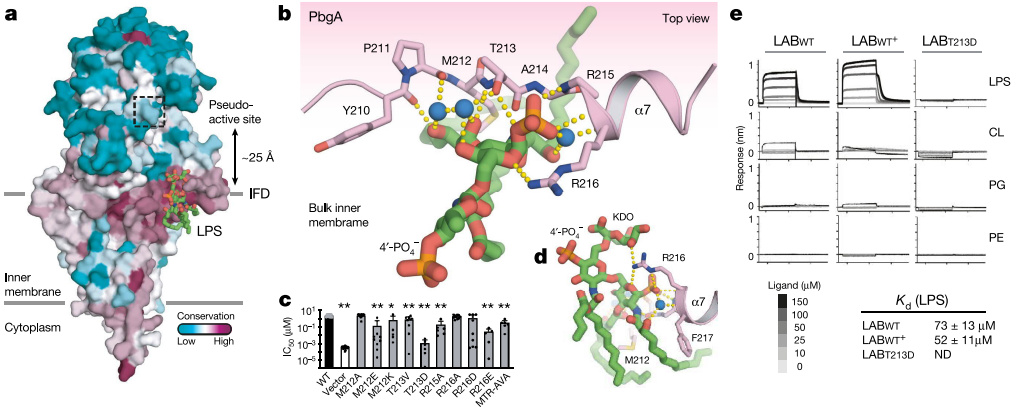

Fig. 3 | The periplasmic lipid A-binding motif of PbgA. a, Conservation analysis calculated across 500 PbgA homologues, surface representation. LPS (sticks) and approximate membrane boundaries are indicated. **b**, Close-up view of the lipid A-binding motif with LPS (green stick representation), water molecules (blue spheres) and most bonding interactions (yellow dashes), shown. **c**, Rifampicin sensitivity of UPEC Δ*pbgA* strains with plasmids expressing wild-type PbgA or mutants. Data are mean ± s.d. from $n = 5$ or more independent experiments per strain. $^{*}P < 0.0041$, $^{**}P < 0.001$, Bonferroni corrected unpaired two-tailed *t*-test. MTR-AVA, M212A/T213V/R216A triple mutant. **d**, As in **b**, but a side view. **e**, Synthetic, biotinylated PbgA-derived lipid A-binding (LAB) peptides transferred into different concentrations of detergent solubilized lipids; binding assessed by interferometry measurements. CL, cardiolipin; PE, phosphatidylethanolamine; PG, phosphatidylglycerol. Data are mean and s.d. and representative of $n = 3$ experiments.

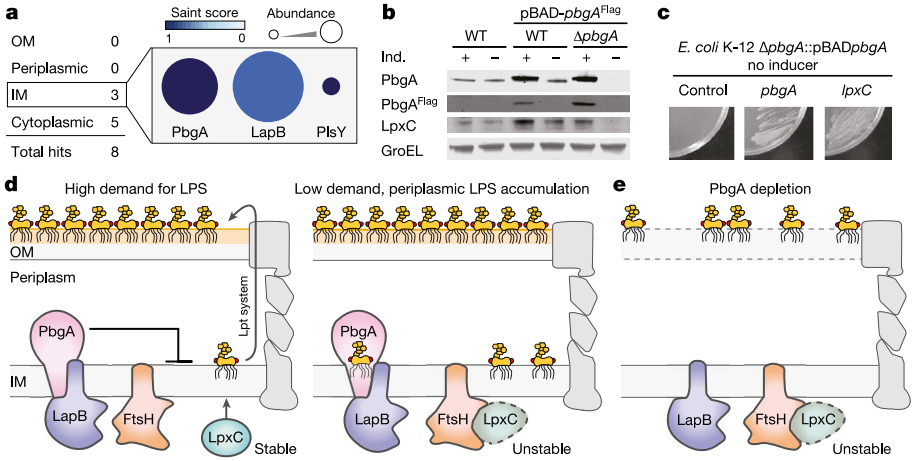

Fig. 4 | PbgA detects periplasmic LPS levels to regulate LpxC stability. **a**, Summary of mass spectrometry analyses following PbgA (endogenous level) immunoprecipitation from *E. coli*. IM, inner membrane; OM, outer membrane. **b**, Western blot of LpxC in the presence or absence of *pbgA*; representative experiment, $n = 3$ or more independent *E. coli* cultures. Ind., inducer. **c**, Growth of conditional PbgA strain with wild-type *pbgA* or *lpxC*; representative plate, $n = 3$ or more independent cultures. **d**, Model of PbgA control of LPS biogenesis and outer membrane integrity. MsbA omitted for clarity and hypothetical cellular states are shown for illustration. When demand for LPS is high, for example, during cell growth (left), the PbgA–LapB complex antagonizes FtsH activity, allowing LpxC to produce LPS precursors. When periplasmic levels of LPS increase, for example, as cells enter stationary phase (right), periplasmic LPS will begin to bind the PbgA–LapB complex, which in turn promotes FtsH degradation of LpxC. **f**, Illustration of the PbgA-depletion phenotype.

Klebsiella pneumoniae, *Acinetobacter baumannii* and *Pseudomonas aeruginosa* (Table 1). Second, consistent with a lipid A-targeting mechanism, growth of the Gram-positive bacterium *S. aureus* that lacks LPS was affected only at very high concentrations (Table 1). Third, when PMX-resistance determinants were introduced into *E. coli*, MICs were unchanged (Table 1, Supplementary Table 9), indicating that LAB peptides and PbgA appear competent to bind unmodified and modified LPS (Fig. 3b, Extended Data Fig. 4c).

The $LAB_{v2.1}$ peptide was bactericidal with time-kill kinetics distinct from PMX antibiotics, potentiated outer membrane-impermeable antibiotics, and synergized with PMX-E (Extended Data Fig. 7b, Supplementary Table 10). Close analogues of $LAB_{v2.1}$ designed to disrupt lipid A interactions had much higher non-specific activity (Extended Data Fig. 7c, d, Supplementary Table 11). Thus, we have discovered a PbgA-inspired class of selective lipid A-binding peptides with activity against Gram-negative pathogens that can overcome modifications that impart PMX resistance.

Table 1 | $LAB_{v2.1}$ peptide exhibits broad-spectrum Gram-negative antibacterial activity

Strain	Phenotype	MICs (μM)[a]
		$LAB_{v2.1}$ YPMXFRRFLEKWGLLR[b]
Escherichia coli ATCC 25922	WT	50
Enterobacter cloacae ATCC 222	WT	12.5
Klebsiella pneumoniae ATCC 43816	WT	100
Acinetobacter baumannii ATCC 19606	WT	12.5
Pseudomonas aeruginosa PA-14	WT	200
Escherichia coli K-12	WT	25
Escherichia coli pmrA^{G53E}	Polymyxin^{R}	12.5
Escherichia coli mcr-1	Polymyxin^{R}	25
*Escherichia coli imp*4213	Permeable	6.25
Staphylococcus aureus USA300	WT	400

[a]MIC is the lowest concentration of compounds that results in complete growth inhibition. [b]N-terminal acetyl, C-terminal amide, 'X' indicates diaminopropionic acid, a non-natural amino acid.

PbgA controls LPS biosynthesis through LpxC

PbgA immunoprecipitation from *E. coli* identified only two cell envelope hits: the inner membrane proteins PlsY and LapB (Fig. 4a, Extended Data Fig. 8a, Supplementary Table 12). We confirmed PbgA interacts proximally with PlsY and LapB, but not FtsH[24], in intact *E. coli* (Extended Data Fig. 8b). PlsY is involved in phospholipid biosynthesis[25] and LapB has a role in coordinating LPS biogenesis[26–28]. Similar to PbgA (Fig. 1), LapB is essential[26] and its mutation leads to defects in the outer membrane barrier, altered cell morphology and cell bursting[28].

LapB promotes degradation of LpxC, which performs the committed step in lipid A biosynthesis, through modulation of the FtsH protease[24,26]. LpxC was not detected after PbgA depletion, and LpxC levels increased when PbgA was overexpressed (Fig. 4b). Thus, PbgA seems to control LPS levels by functioning as a negative regulator of LapB to ultimately dictate LpxC levels. Accordingly, overexpression of *lpxC* suppressed *pbgA* essentiality, whereas *lapB* overexpression did not (Fig. 4c, Extended Data Fig. 8c).

PbgA is uniquely positioned to detect LPS within the periplasmic leaflet of the *E. coli* inner membrane[10–12] (Fig. 4d). Notably, the PbgA T213D mutant expected to disrupt LPS binding increased LpxC levels and disturbed outer membrane homeostasis (Fig. 3c, Extended Data Fig. 8d). Depletion of periplasmic LPS using an MsbA inhibitor[29] increased levels of LpxC, whereas increasing periplasmic LPS through LptD depletion[30] decreased LpxC levels (Extended Data Fig. 8e, f). We conclude that direct periplasmic sensing of LPS by PbgA controls outer membrane homeostasis through LapB- and FtsH-mediated regulation of LpxC levels.

Discussion

PbgA lacks structural similarity to known transporters or phospholipid-binding proteins. We find that cardiolipin does not co-purify with PbgA, does not bind to the isolated IFD-derived peptide, and is not required to maintain outer membrane integrity in *E. coli*. Our high-resolution crystallographic data permit re-evaluation of a modest PbgA structure[7], which leads to the conclusion that lipid A, not cardiolipin, is bound along the IFD (Extended Data Fig. 9). Moreover, LPS co-purifies with PbgA and binds to the isolated IFD-derived peptide, and lipid A levels are reduced after PbgA depletion, concomitant with a defect in the outer membrane barrier.

PbgA presents a new paradigm in selective lipid recognition as it does not seem to require divalent cations or basic residues to bind lipid A[4,31]. By targeting only a single phospho-GlcNAc unit, PbgA distinguishes itself from known LPS receptors[32], LPS transporters[29,33] and outer membrane proteins[34,35] that exploit the lipid A disaccharide (Extended Data Fig. 10). We leveraged these observations to discover selective LPS-binding peptides that can kill clinically relevant *E. coli*, *E. cloacae*, *K. pneumoniae*, *A. baumannii* and *P. aeruginosa* bacteria in vitro (Table 1), including PMX-resistance strains. Further improvements of $LAB_{v2.1}$ peptide potency, selective outer membrane partitioning, and activity in serum will enable assessment in preclinical infection models.

Exactly how LPS synthesis and transport are coordinated to maintain outer membrane integrity has remained unclear[10–12], but here we reveal the structural basis of an essential LPS–PbgA interaction within the inner membrane. In our model, when cellular demand for LPS is high, LpxC must be stable and active, leading to positive LPS flux (Fig. 4d, left). Under this condition, PbgA exists bound to LapB in an LPS-free state and antagonizes FtsH proteolytic activity. When periplasmic levels of LPS increase, LPS binds to PbgA, altering PbgA–LapB interactions, which promotes activation of FtsH to degrade LpxC (Fig. 4d, right). Overall, LPS levels on the periplasmic leaflet of the inner membrane control the rate of LPS synthesis through direct binding or unbinding to PbgA, functioning as a rheostat to dictate LpxC levels (Fig. 4d).

Our model rationalizes the PbgA depletion phenotype (Fig. 4e) and indicates that disruption of the periplasmic LPS–PbgA interaction may represent a compelling antibacterial strategy. However, key questions persist. LapB remains associated with the PbgA–TMD after deletion of the IFD and periplasmic domain, or when disruptive mutations are introduced into the lipid A-binding motif, which suggests that LapB and PbgA form a constitutive complex (Extended Data Fig. 8g–i). Thus, how LPS binding alters the LapB–PbgA interaction and modulation of FtsH activity remains unknown. A defect in the outer membrane exists in the PbgA–TMD-only strain, indicating altered LPS levels due to an inability to sense LPS, but why this mutant remains viable is not clear[15,18] (Extended Data Fig. 8g–i). A putative phosphatidylethanolamine bound within a conserved cleft on PbgA (Extended Data Fig. 2b) will certainly fuel speculation of a cryptic activity in the TMD[7,14] and other connections to phospholipid biology[6,17,18] (Extended Data Fig. 8j, k). Overall, we have characterized PbgA as a key regulator of LPS biogenesis and outer membrane integrity through the direct detection of LPS on the periplasmic leaflet of the inner membrane, and also present opportunities for future antibiotic discovery.

1. Whitfield, C. & Trent, M. S. Biosynthesis and export of bacterial lipopolysaccharides. *Annu. Rev. Biochem.* **83**, 99–128 (2014).
2. Shrivastava, R. & Chng, S. S. Lipid trafficking across the Gram-negative cell envelope. *J. Biol. Chem.* **294**, 14175–14184 (2019).
3. Parrillo, J. E. Pathogenetic mechanisms of septic shock. *N. Engl. J. Med.* **328**, 1471–1477 (1993).
4. Pristovsek, P. & Kidric, J. Solution structure of polymyxins B and E and effect of binding to lipopolysaccharide: an NMR and molecular modeling study. *J. Med. Chem.* **42**, 4604–4613 (1999).
5. Poirel, L., Jayol, A. & Nordmann, P. Polymyxins: antibacterial activity, susceptibility testing, and resistance mechanisms encoded by plasmids or chromosomes. *Clin. Microbiol. Rev.* **30**, 557–596 (2017).
6. Dalebroux, Z. D. et al. Delivery of cardiolipins to the *Salmonella* outer membrane is necessary for survival within host tissues and virulence. *Cell Host Microbe* **17**, 441–451 (2015).
7. Fan, J., Petersen, E. M., Hinds, T. R., Zheng, N. & Miller, S. I. Structure of an inner membrane protein required for PhoPQ-regulated increases in outer membrane cardiolipin. *MBio* **11**, e03277-19 (2020).
8. Dong, H. et al. Structural insights into cardiolipin transfer from the Inner membrane to the outer membrane by PbgA in Gram-negative bacteria. *Sci. Rep.* **6**, 30815 (2016).
9. Rossi, R. M., Yum, L., Agaisse, H. & Payne, S. M. Cardiolipin synthesis and outer membrane localization are required for *Shigella flexneri* virulence. *MBio* **8**, e01199-17 (2017).
10. Guest, R. L., Samé Guerra, D., Wissler, M., Grimm, J. & Silhavy, T. J. YejM Modulates activity of the YciM/FtsH protease complex to prevent lethal accumulation of lipopolysaccharide. *MBio* **11**, e00598-20 (2020).
11. Fivenson, E. M. & Bernhardt, T. G. An essential membrane protein modulates the proteolysis of LpxC to control lipopolysaccharide synthesis in *Escherichia coli*. *MBio* **11**, e00939-20 (2020).
12. Nguyen, D., Kelly, K., Qiu, N. & Misra, R. YejM controls LpxC levels by regulating protease activity of the FtsH/YciM complex of *Escherichia coli*. *J. Bacteriol.JB*. 00303-20 (2020).
13. Sorensen, P. G. et al. Regulation of UDP-3-O-[*R*-3-hydroxymyristoyl]-*N*-acetylglucosamine deacetylase in *Escherichia coli*. The second enzymatic step of lipid a biosynthesis. *J. Biol. Chem.* **271**, 25898–25905 (1996).
14. Gabale, U., Palomino, P. A. P., Kim, H., Chen, W. & Ressl, S. New functional identity of the essential inner membrane protein YejM: the cardiolipin translocator is also a metalloenzyme. Preprint at https://www.biorxiv.org/content/10.1101/2020.02.13.947838v1 (2020).
15. Hirvas, L., Nurminen, M., Helander, I. M., Vuorio, R. & Vaara, M. The lipid A biosynthesis deficiency of the *Escherichia coli* antibiotic-supersensitive mutant LH530 is suppressed by a novel locus, ORF195. *Microbiology* **143**, 73–81 (1997).
16. Nurminen, M., Hirvas, L. & Vaara, M. The outer membrane of lipid A-deficient *Escherichia coli* mutant LH530 has reduced levels of OmpF and leaks periplasmic enzymes. *Microbiology* **143**, 1533–1537 (1997).
17. Cian, M. B., Giordano, N. P., Masilamani, R., Minor, K. E. & Dalebroux, Z. D. *Salmonella enterica* Serovar Typhimurium uses PbgA/YejM to regulate lipopolysaccharide assembly during bacteremia. *Infect. Immun.* **88**, e00758-19 (2019).
18. De Lay, N. R. & Cronan, J. E. Genetic interaction between the *Escherichia coli* AcpT phosphopantetheinyl transferase and the YejM inner membrane protein. *Genetics* **178**, 1327–1337 (2008).
19. Jia, W. et al. Lipid trafficking controls endotoxin acylation in outer membranes of *Escherichia coli*. *J. Biol. Chem.* **279**, 44966–44975 (2004).
20. Qiu, N. & Misra, R. Overcoming iron deficiency of an *Escherichia coli tonB* mutant by increasing outer membrane permeability. *J. Bacteriol.* **201**, e00340-19 (2019).
21. Fronzes, R. et al. Structure of a type IV secretion system core complex. *Science* **323**, 266–268 (2009).
22. Lu, D. et al. Structure-based mechanism of lipoteichoic acid synthesis by *Staphylococcus aureus* LtaS. *Proc. Natl Acad. Sci. USA* **106**, 1584–1589 (2009).
23. Anandan, A. et al. Structure of a lipid A phosphoethanolamine transferase suggests how conformational changes govern substrate binding. *Proc. Natl Acad. Sci. USA* **114**, 2218–2223 (2017).
24. Ogura, T. et al. Balanced biosynthesis of major membrane components through regulated degradation of the committed enzyme of lipid A biosynthesis by the AAA protease FtsH (HflB) in *Escherichia coli*. *Mol. Microbiol.* **31**, 833–844 (1999).
25. Yoshimura, M., Oshima, T. & Ogasawara, N. Involvement of the YneS/YgiH and PlsX proteins in phospholipid biosynthesis in both *Bacillus subtilis* and *Escherichia coli*. *BMC Microbiol.* **7**, 69 (2007).
26. Klein, G., Kobylak, N., Lindner, B., Stupak, A. & Raina, S. Assembly of lipopolysaccharide in *Escherichia coli* requires the essential LapB heat shock protein. *J. Biol. Chem.* **289**, 14829–14853 (2014).
27. Mahalakshmi, S., Sunayana, M. R., SaiSree, L. & Reddy, M. yciM is an essential gene required for regulation of lipopolysaccharide synthesis in Escherichia coli. *Mol. Microbiol.* **91**, 145–157 (2014).
28. Nicolaes, V. et al. Insights into the function of YciM, a heat shock membrane protein required to maintain envelope integrity in *Escherichia coli*. *J. Bacteriol.* **196**, 300–309 (2014).
29. Ho, H. et al. Structural basis for dual-mode inhibition of the ABC transporter MsbA. *Nature* **557**, 196–201 (2018).
30. Wu, T. et al. Identification of a protein complex that assembles lipopolysaccharide in the outer membrane of *Escherichia coli*. *Proc. Natl Acad. Sci. USA* **103**, 11754–11759 (2006).
31. Lemmon, M. A. Membrane recognition by phospholipid-binding domains. *Nat. Rev. Mol. Cell Biol.* **9**, 99–111 (2008).
32. Park, B. S. et al. The structural basis of lipopolysaccharide recognition by the TLR4–MD-2 complex. *Nature* **458**, 1191–1195 (2009).
33. Li, Y., Orlando, B. J. & Liao, M. Structural basis of lipopolysaccharide extraction by the $LptB_2FGC$ complex. *Nature* **567**, 486–490 (2019).
34. Ferguson, A. D., Hofmann, E., Coulton, J. W., Diederichs, K. & Welte, W. Siderophore-mediated iron transport: crystal structure of FhuA with bound lipopolysaccharide. *Science* **282**, 2215–2220 (1998).
35. Arunmanee, W. et al. Gram-negative trimeric porins have specific LPS binding sites that are essential for porin biogenesis. *Proc. Natl Acad. Sci. USA* **113**, E5034–E5043 (2016).

Bacterial strains and plasmids

To generate pBAD-*pbgA*, *pbgA* was amplified from uropathogenic *E. coli* (UPEC CFT073) and cloned into pBAD vector using Gibson assembly according to manufacturer's instructions (New England Biolabs). Mutations in *pbgA* were created using QuikChange II XL site-directed mutagenesis kit (Agilent Technologies) and confirmed by PCR and DNA sequencing.

Mutant strains were created using λ Red recombination[36]. In brief, the kanamycin or gentamicin cassette from pKD4 was amplified with primers containing ~50 bp nucleotide homology extensions to the gene of interest. The linear product was transformed into the appropriate background strain containing pSIM18[37], recovered for 4 h at 37 °C, and selected on medium containing 50 μg ml^{-1} kanamycin or 12.5 μg ml^{-1} chloramphenicol or 10 μg ml^{-1} gentamicin, as appropriate. Mutations were confirmed by PCR and sequencing. Construction of the UPEC-Δ*pbgA* and K-12-Δ*pbgA* strains resulted in single clones and the *pbgA* deletions were confirmed by PCR. Because *pbgA* is reported to be essential[18], we isolated genomic DNA using the Blood and Cell Culture DNA Maxi kit (Qiagen) and sequenced it using the Illumina HiSeq 2000 platform to identify the suppressor. Paired-end 75 bp reads were aligned to the *E. coli* CFT073 genome using GSNAP version 2013-10-10 with the following parameters: -M 2 -n 10 -B 2 -i 1–pairmax-dna = 1000–terminal-threshold = 1000–gmap-mode = none–clip-overlap. Variant calling was performed using an in-house bioinformatics pipeline using R and Bioconductor packages, GenomicRanges[38], GenomicAlignments[38], VariantTools, and gmapR, with a required base quality score for variant tallying of 30. No single-nucleotide variants or indels were found, but mapping confirmed this strain lacked the *pbgA* gene and identified a large (~569 kb) genomic duplication that straddles the origin (nucleotide positions 1-257,753 and 4,930,864-5,242,376). The mechanism of *pbgA* suppression in this strain has not yet been determined, but *acpT*, a reported multi-copy suppressor of Δ*pbgA*[18], is not duplicated in UPEC Δ*pbgA*.

The conditional *pbgA* strain, Δ*pbgA*::pBAD*pbgA*, was created by inserting pBAD*pbgA* at the *attB* site in BW25113 followed by deletion of the native copy of *pbgA*[36,39]. In brief, *pbgA* was cloned into pBAD28 using standard methods. pBAD*pbgA* was amplified from pBAD28-*pbgA* and sub-cloned into pLDR9. pLDR9-pBAD*pbgA* was digested with NotI, ligated, and transformed into BW25113 expressing pLDR8. PCR and DNA sequencing confirmed insertion of pBAD*pbgA* at the *attB* site. After integration of pBAD*pbgA*, the native copy of *pbgA* was deleted using λ Red recombination as described above.

The triple Δ*clsABC* mutant was constructed by sequentially introducing each individual *cls* deletion from the Keio collection[40] into *E. coli* BW25113 by P1*vir* transduction using standard procedures[41]. Deletions were confirmed by PCR.

pFhuAΔC/Δ4L (pGNE30) was constructed by synthesizing the *fhuA* coding sequence lacking the N-terminal cork domain, Δ1-160, and extracellular loops L3, L4, L5 and L11[42]. *fhuA*ΔcΔ4L was amplified with primers N3P-105 (encoding the *bla* constitutive promoter, ribosome binding site, and AUG start codon from pUC19 (New England BioLabs) and N3P-107, and cloning into pACYC184 with BamHI and HindIII (New England BioLabs). Constitutive expression of *fhuA*ΔC/Δ4L in wild-type *E. coli* results in increased sensitivity to vancomycin and rifamycin.

For complementation and suppression of *E. coli* K-12 Δ*pbgA*::*pBADpbgA*, ASKA (GFP-) plasmids ECK1275 (*lapB*), ECK4026 (*malE*; as control) ECK2182 (*pbgA*), ECK3049 (*plsY*), ECK3459 (*acpT*), ECK2561 (*acpS*), ECK0097 (*lpxC*) were used[43]. Colonies were selected on LB agar plus 25 μg ml^{-1} chloramphenicol and 0.02% arabinose. To test for complementation or suppression, plasmid-containing strains were streaked onto LB agar plates with 25 μg ml^{-1} chloramphenicol but without IPTG as leakiness of the promoter was sufficient to complement (*pbgA)* and higher induction was lethal, or with 20 or 50 μM IPTG (*lpxC*), 50 or 100 μM IPTG (*acpT* and *acpS*) or with all previous listed conditions (*lapB* and *plsY*). For western blot analysis, bacteria scraped from LB agar plates with arabinose were diluted to OD_{600} of 0.025 in LB and arabinose or IPTG conditions as above, grown at 37 °C with aeration, and collected as described below. All strains, plasmids and primers used in this study are listed in the Supplementary Tables 13–15.

Bacterial growth conditions

LB (broth or agar) or Mueller Hinton II cation-adjusted broth (MHB II, BBL 212322) was prepared according to manufacturer's instructions and supplemented with arabinose at 0.02% or at indicated concentrations in figure legends. Bacterial cultures were grown at 37 °C, static, with humidity in 96-well plates for time course and sensitivity assays. To deplete PbgA from Δ*pbgA*::pBAD*pbgA* for western blot analysis, bacteria were grown at 37 °C for around 5 h with dilution to maintain log phase (~8–10 generations), in shaking liquid culture. To deplete PbgA for growth curves, cultures were grown statically at 37 °C and back-diluted 1/10 to maintain logarithmic growth. When appropriate, medium was supplemented with kanamycin (50 μg ml^{-1}), carbenicillin (50 μg ml^{-1}), chloramphenicol (12.5 or 25 μg ml^{-1}), hygromycin (200 μg ml^{-1}), and/or gentamicin (10 μg ml^{-1}). To deplete LptD from *E. coli* K-12 Δ*lptD*::pBAD-*lptD*, bacteria were scraped from LB agar with 0.02% arabinose, diluted into LB broth to an OD_{600} of 0.05, supplemented with 0.02, 0.002 or 0.0002% arabinose, and grown to log-phase at 37 °C with shaking. Bacterial cells were obtained as described below.

Rifampicin-sensitivity assay

For *E. coli* K-12 Δ*pbgA*::pBAD-*pbgA*, bacteria were grown on LB agar plates containing 0.02% arabinose overnight at 37 °C. Cells were scraped from the plate into LB broth, diluted to OD_{600} 0.025, grown to mid-log phase (2.5 h, or approximately 4 generations) at 37 °C, back-diluted in fresh LB broth to OD_{600} 0.025, and grown to mid-log phase again to deplete PbgA accumulated during overnight growth. Rifampicin assay plates were made by serially diluting rifampicin (Sigma) stock (10 mM in DMSO) in LB medium in clear round-bottom 96-well plates (Costar). Bacteria were added to each well to a final OD_{600} 0.01. Plates were incubated at 37 °C statically and OD_{600} read at 4–6 h.

For UPEC strains, each *pbgA*-encoding pBAD28 plasmid was freshly transformed into UPEC-Δ*pbgA* by standard methods and plated onto LB agar plates containing 0.2% glucose and 50 μg ml^{-1} carbenicillin and incubated overnight at 37 °C. Three isolated colonies were picked and re-streaked onto LB agar plus 0.2% glucose and 50 μg ml^{-1} carbenicillin. A single isolated colony from each plate was heavy-streaked onto LB agar containing 50 μg ml^{-1} carbenicillin. Uninduced expression of *pbgA* from the arabinose-inducible promoter was sufficient to complement Δ*pbgA* and PbgA protein levels for each mutant were confirmed by western blot analysis (Extended Data Fig. 6a). Bacteria were scraped from the plate into LB media, diluted, and added to the rifampicin assay plate as described above. Dose–response curves were fit using PRISM software using '[inhibitor] vs response - variable slope' analysis. IC_{50} values from at least four biological replicates were averaged and standard deviation calculated. Values were compared with unpaired two-tailed *t*-test in PRISM and corrected for multiple comparisons (Bonferroni).

Western blot analysis

For UPEC strains, an equivalent of 0.5 OD_{600} bacterial cells were collected by centrifugation and frozen. Pellet was thawed, suspended in PBS and 1× NuPAGE LDS sample buffer (Invitrogen), incubated 20 min, and bath sonicated 10 min in thin-walled sample tubes. Samples were separated on 4–12% NU-PAGE gel (Invitrogen) and transferred to nitrocellulose using the iBLOT2 system (Thermo Fisher Scientific). Nitrocellulose was blocked (PBS with 5% non-fat milk, 0.05% Tween 20) for 1 h and probed for PbgA–Flag overnight at 4 °C with mouse anti-Flag antibody (Cell Signaling Technology) at 1:500–1:1,000 in PBS. A horseradish peroxidase (HRP)-conjugated secondary antibody

(GE Healthcare) at 1:5,000 dilution was incubated with the nitrocellulose for 1 h in 5% non-fat milk in TBS plus 0.05% Tween 20. Between all steps the membrane was washed three times with TBS plus 0.05% Tween 20 and blots were developed using ECL Prime Western Blotting Detection Reagent (Amersham). Blots were stripped with Restore PLUS Western Blot stripping buffer (Thermo Scientific), washed with PBS three times, blocked and probed as described above but with 1:25,000 rabbit anti-GroEL (Enzo) for 1 h.

For all other western blots, an equivalent of OD_{600} of 0.5 bacterial cells from shaking liquid cultures or scraped from LB agar plates were collected by centrifugation and frozen. Pellets were thawed, suspended in 1× LICOR protein sample buffer with 4% β-mercaptoethanol, incubated 10 min at room temperature and then for 5–10 min at 95 °C. Samples were separated on 4–12%, 10%, or 12% NU-PAGE gels (Invitrogen) and transferred to nitrocellulose using the iBLOT2 system (Thermo-Fisher Scientific). Nitrocellulose was blocked in Odyssey PBS blocking buffer (LICOR) for 1–3h at room temperature. Primary antibody incubations were performed at 4 °C overnight at indicated concentrations. Rabbit anti-LpxC (LSBio) was used at 1:5,000–1:10,000 and anti-PbgA monoclonal antibody (7E7, described further below) was used at 1:500, mouse anti-Flag (Cell Signaling Technologies) at 1:500, rabbit anti-GroEL at >1:10,000, human anti-LptD at 1 μg ml^{-1}, all in PBS overnight at 4 °C. After washing membranes three times with TBS plus 0.05% Tween 20, membranes were incubated in Odyssey blocking buffer plus a 1:10,000 dilution of LI-COR goat anti-mouse, anti-rabbit, or anti-human secondary antibodies (IRDye 680RD, IRDye 800CW) and imaged on a LI-COR Odyssey LCx scanner. Antibody information and unprocessed, uncropped western blot gel images are provided in Supplementary Fig. 1.

MIC and time-kill assays

LAB peptides (Smartox Biotechnology, CPC Scientific, ABclonal, standard solid-phase peptide synthesis) at 10 mM in 50 mM Tris, pH 8, and 100 mM NaCl were diluted in MHB II cation adjusted broth (800 μM top concentration) or LB. Where indicated, EDTA was added to a final concentration of 0.5 mM. For modified MIC assays, log phase cultures growing in LB were diluted to OD_{600} of 0.0002 in a final volume of 10 μl in 384-well plates (Corning). Plates were incubated statically at 37 °C and OD_{600} was read after 20 h on EnVision plate reader. For the potentiation MIC assay, log-phase cultures grown in LB were diluted to an OD_{600} of 0.0002 in a final volume of 50 μl in 96-well plate (Corning) with concentration of peptide and antibiotic as indicated in tables. Growth (OD_{600}) was measured after static overnight incubation at 37 °C with humidity using a SpectraMax M5 plate reader.

For the time-kill assay, three independent cultures of wild-type *E. coli* (ATCC 25922) were grown to log-phase before being diluted into indicated concentration of peptide relative to the MIC found in Table 1 (that is, 1× MIC = 50 μM) or polymyxin B and incubated at 37 °C, static with humidity. At times indicated, sample was taken, diluted in PBS, and plated on LB agar. CFUs were counted after overnight incubation.

For experiments with MsbA inhibitor[44], *E. coli imp*4213 was grown to an OD_{600} of 0.3, split into three separate cultures (1 μM G913, 4 μM G913, or an equal volume of DMSO), and incubated at 37 °C for 1h. Bacterial cells were collected and processed for western blot analysis with anti-LpxC and anti-GroEL antibodies as described.

Red blood cell lysis assay

Collection of human blood samples from volunteers was through the Genentech Samples for Science Program and carried out under protocols approved by the Western Institutional Review Board (protocol number CEHS-CP 307.2, IRB tracking number 20080040). No personal or medical history was specified, provided or collected for volunteers.

Peptides were diluted in PBS in a 96-well clear round bottom plate at two times the final concentration in 60 μl per well. Whole heparinized human blood was diluted to 4% in PBS and 60 μl added to the diluted peptides such that the final blood concentration was 2%. Plates were incubated at 37 °C, static with humidity for 30 min or overnight then centrifuged at 600*g* for 3 min, 60 μl of supernatant was removed to a clear flat bottom plate and OD405 read on a SpectraMax M5 plate reader (Molecular Devices).

Bacterial two-hybrid

The bacterial two-hybrid assay used the Bacterial Adenylate Cyclase Two-Hybrid (BACTH) System Kit (Euromedex) and is based on published methods[45,46]. Fusions were made using BACTH plasmids encoding T25 or T18 adenylate cyclase domains to the N- or C-terminal where appropriate to ensure domains were present on the cytoplasmic side of the inner membrane. pKT25-*pbgA* was tested against the following baits: pUT18-*lapB*, *plsY* and *ftsH* and pUT18C-*hisM* and *pbgA*. pKT25-*pbgA* truncated, EptA-TM swap, or point mutant variants were tested with pUT18-*lapB*. The T25 plasmid (pKT25-*pbgA*) and a T18 plasmid were co-transformed into an adenylate cyclase-deficient *E. coli* strain (DHM1) and grown for 1–2 days at 30 °C on LB agar plate with 50 μg ml^{-1} kanamycin, 50 μg ml^{-1} carbenicillin, and 40 μg ml^{-1} X-gal. Interacting proteins that re-constituted the CyaA adenylate cyclase active site by bringing T25 and T18 together formed blue colonies while partners that did not interact led to white colonies. At least three single isolated colonies were re-streaked onto fresh agar plates to confirm the phenotype.

Ethics statement

All mice used in the in vivo studies were housed and maintained at Genentech in accordance with American Association of Laboratory Animal Care guidelines. All experimental studies were conducted under protocols approved by the Institutional Animal Care and Use Committee of Genentech Lab Animal Research in an Association for Assessment and Accreditation of Laboratory Animal Care International (AAALAC)-accredited facility in accordance with the Guide for the Care and Use of Laboratory Animals and applicable laws and regulations.

In vivo infections

For the in vivo infection model, 7-week-old A/J mice (Jackson Laboratory) were rendered neutropenic by peritoneal injection of two doses of cyclophosphamide (150 mg kg^{-1} on day −4 and 100 mg kg^{-1} on day −1). On day 0, mice were infected by intravenous injection through the tail vein of 1×10^6 CFU mid-exponential-phase bacteria diluted in PBS. At 30 min and 24 h after infection, bacterial burdens in the liver and spleen were determined by serial dilutions of tissue homogenates on LB plates. Samples sizes were not predetermined, data were not blinded and experiments were not randomized.

For the thigh infection model, 6-week-old CD1 mice (Charles River Laboratories) were rendered neutropenic by peritoneal injection of 2 doses of cyclophosphamide (150 mg kg^{-1} on day −5 and 100 mg kg^{-1} on day −2). On day 0, mice were infected by intramuscular injection in the thigh muscle of 2×10^4 CFU mid-exponential-phase bacteria diluted in PBS. At 24 h after infection, bacterial burdens in the thigh muscle were determined by serial dilutions of tissue homogenates on LB plates. Samples sizes were not predetermined and data were not blinded.

Extraction and detection of membrane phospholipids

Membrane phospholipids were extracted from outer membrane vesicles using a modified Bligh–Dyer protocol[47] as follows: outer membrane vesicles were prepared from (1×10^6 cells) and suspended in 0.9 ml water, 2 ml methanol (Thermo Fisher Scientific) and 0.9 ml dichloromethane (Acros Organics) were added and vortexed, and the organic layer was removed. The process was repeated and extracts were combined and dried under steady nitrogen flow. Dried residue was reconstituted in 50 μl of 50:50 dichloromethane:methanol with 10 mM ammonium acetate and subjected to LC–MS/MS analysis. Then, 30 μl of sample was injected on a MetaSil AQ C18 column (150 × 2.0 mm, 3.0 μm, Agilent) on a HPLC system (Shimadzu). The temperatures of the column

oven and autosampler were set at 45 °C and 15 °C, respectively. Flow rate was 0.3 ml min^{-1} and the gradient was held at 40% mobile phase A (methanol containing 10 mM ammonium acetate) for the initial 3 min. Mobile phase B (dichloromethane with 10 mM ammonium acetate) was increased to 85% over 9 min, then further increased to 95% in 30 s and maintained at 95% for 3 min before returning to initial conditions for re-equilibration and subsequent injections. The HPLC was coupled to a 6500+ QTRAP mass spectrometer (Sciex) operated under positive ionization mode with the following source settings: turbo-ion-spray source at 350 °C under N_2 nebulization at 20 psi, N_2 heater gas at 10 psi, curtain gas at 30 psi, collision-activated dissociation gas pressure was held at medium, turbo ion-spray voltage at 5,500 V, declustering potential at 20 V, entrance potential at 10 V.

Bacterial membrane lipids phosphatidylethanolamine, phosphatidylcholine and cardiolipin were detected by characteristic head group ions present upon fragmentation in either precursor ion scan mode or neutral loss. For phosphatidylethanolamine and phosphatidylcholine, ions were scanned for neutral loss in positive polarity for losses of 141 Da and 184 Da, respectively. Cardiolipin was detected through precursor ion scan in negative mode with a precursor of 391.5 Da. Collision energies were set to 24 V (phosphatidylethanolamine and phosphatidylcholine), and −65 V for cardiolipin. Other parameters were as follows (flipped for negative polarity): CXP 16, EP 10, IS 4500, CUR 20 at temperature (TEM) of 150 °C.

Time-lapse microscopy

E. coli K-12 Δ*pbgA*::pBAD-*pbgA* with arabinose-inducible *pbgA* grown overnight on LB with 0.02% arabinose was inoculated into LB lacking arabinose and grown for 4.5h to deplete PbgA. Cells were maintained in log phase until spotting onto a glass bottom culture dish (MatTek Corporation) and overlaid with a 1% agarose pad made with LB or MHB media. Imaging was performed on a Nikon Eclipse TE inverted fluorescence microscope with a 100× (NA 1.30) oil-immersion objective (Nikon Instruments). Images were collected every 2 min using an Andor DR electron-multiplying CCD camera (Andor Technology) using NIS-Elements software (Nikon Instruments). Cells were maintained at 37 °C during imaging with a temperature-controlled environmental chamber (World Precision Instruments). A representative image of the morphology changes seen in the time course (time taken indicated in figure legend) and in the >3 biological replicates is shown in the figure.

Recombinant protein expression and purification

Full-length (residues 1–586) of *E. coli* and *S. typhimurium* PbgA followed by a TEV cleavage site, 2×Flag tag and a hexahistidine tag at the C terminus were cloned into a modified pET52b vector. Proteins were expressed in *E. coli* BL21-Gold(DE3) for 48 h in TB autoinduction medium at 17 °C. Fifty grams of cell pellet was resuspended in 250 ml of 50 mM Tris pH 8, 300 mM NaCl, 1 μg ml^{-} benzonase, 1 mM PMSF and Roche protease inhibitor tablets. Cells were lysed by sonication and PbgA were subsequently solubilized by addition of either 1% (w/v) LMNG or 1% (wt/v) dodecyl maltoside (DDM) for 2 h at 4 °C under gentle agitation. Insoluble debris was pelleted by centrifugation at 18,000 rpm for 1 h, and the supernatant containing the solubilized protein was collected for affinity purification by batch-binding to 20 ml of M2-agarose Flag resin (Sigma) for 2 h at 4 °C. Unbound proteins were washed with 10 column volumes of purification buffer (50 mM Tris pH 8, 300 mM NaCl, 0.025% (w/v) LMNG or DDM) and eluted with 5 column volumes of purification buffer supplemented with 150 μg ml^{-1} Flag peptide (Sigma). The eluate was collected and concentrated with 100 kDa MWCO concentrators to 1 mg ml^{-1} before tag removal by TEV cleavage overnight at 4 °C. PbgA was then concentrated to 4 mg ml^{-1}, supplemented with 1 mM $NiCl_2$, and injected onto a Superdex S200 Increase 10/300 column attached to an AKTA system (GE Healthcare) for size-exclusion chromatography into crystallization or SEC-MALS buffer (20 mM sodium citrate pH 5, 200 mM NaCl, 0.025% LMNG or DDM). Elution fractions corresponding to monomeric PbgA in LMNG were pooled and concentrated to 40 mg ml^{-1} for crystallization. For the preparation of *E. coli* MsbA (residues 1–582) and *E. coli* Lnt (residues 1–594), constructs were similarly cloned and proteins were expressed and purified in LMNG using the above protocol. For the purification of LPS-free MsbA ($MsbA_{293}$), *E. coli* MsbA (residues 1–582) was cloned into a pRK vector behind a CMV promoter and transiently transfected into Expi293 cells (human embryonic kidney cells; Thermo Fisher Scientific, A14527) using standard protocols. This cell line was not authenticated, but tested negative for mycoplasma contamination. Following expression in this eukaryotic host, purification of $MsbA_{293}$ was carried out as described above using an endotoxin-free AKTA system.

Crystallization, data collection and structure determination

Crystal screens in LCP were set up using 40 mg ml^{-1} PbgA and a monoolein (Sigma): phosphatidylethanolamine (*E. coli* PE, Avanti Polar Lipids) 99.5:0.5% m/m mixture at 40% hydration. Protein–lipid mixes were prepared at room temperature as previously described[48] and crystals grew in 50 nl drops surrounded by 800 nl reservoir solution. Rounds of optimization in MemMeso HT screens (Molecular dimensions) yielded the best-diffracting PbgA crystals that were obtained in a buffer containing 0.1 M Tris pH 8.0, 0.2 M ammonium sulfate, 40% PEG200 at 4 °C, and grew to their maximum size in approximately 20 days. Crystals were flashed-frozen without further cryoprotection for screening. 180° of X-ray diffraction data were collected from a single crystal at the Stanford Synchrotron Radiation Lightsource beamline SSRL12-2 at 100 K, and integrated and scaled using HKL2000[49]. Diffraction from PbgA crystals was anisotropic; however, treatment through the anisotropy server did not indicate severe anisotropy (https://services.mbi.ucla.edu/anisoscale/)[50], nor lead to noticeable improvement in map quality, so it was not applied. To provide a view of the available diffraction data: quality and completeness across 3 different resolution zones (that is, 2.34–2.3; 2.03–2; and 1.88–1.85) are provided in Supplementary Table 2, where completeness is 62%, $CC_{1/2}$ 0.74, I/σ1.7 and redundancy 1.9 at 2.0 Å resolution. PbgA crystallized in the *C*2 space group with one monomer in the asymmetric unit. The PbgA structure was determined by molecular replacement using PHASER[51] with the PbgA periplasmic domain search model (PDB: 5I5H). Following rigid-body refinement of the periplasmic domain template, clear electron density was visible for the transmembrane domain. The model was completed manually and rebuilt through iterative refinement and omit maps using COOT[52] and PHENIX[53]. Secondary structure restraints were initially applied during refinement but relaxed, and TLS parameters were also employed at late stages in refinement[54]. LPS was modelled only at very late stages of refinement after all protein, other lipids, and most solvent molecules were accounted for. Because reasonable completeness and data quality were available to 1.85 Å, the structure with ligands were refined against all available data until the last round of refinement, where the resolution was cut back to 2.0 Å (Supplementary Table 2). Conservation analysis was performed with Consurf[55], structural homologues were searched for and identified using the Dali server[56], and all structural figures were generated using PyMOL[57]. Where shown, our density maps were calculated to 2.0 Å with $F_o - F_c$ maps calculated before the inclusion of LPS into the refined model to avoid introducing any bias from this ligand.

Crystallization, data collection and structure determination by serial femtosecond X-ray crystallography

PbgA microcrystals were prepared by optimizing the composition of the precipitant solution the macrocrystals were grown in, eventually yielding 5–10 μm crystals that formed in 0.1 M Tris pH 8.4, 0.2 M ammonium sulfate, 24% PEG200 at 20 °C after 48 h incubation. Crystals were then grown in syringes and prepared for serial femtosecond X-ray crystallography data collection as previously described[58]. LCP-SFX data collection was performed using the CXI instrument at the Linac

Coherent Light Source at SLAC National Accelerator Laboratory. 7.9 MAG was added to the PbgA microcrystals LCP medium at around 30% final concentration, and the mixture was injected at a flow rate of approximately 0.400 µl min^{-1} into a vacuum chamber with a 50 µm diameter nozzle. The X-ray free-electron laser was operated at a repetition rate of 120 Hz at a wavelength of 1.3 Å (9.5 keV), delivering focused X-ray pulses of ~40-fs duration with a FWHM of approximately 1.5 µm in diameter. A total of 556,136 detector frames (corresponding to approx. 80 min of data collection) resulted in an average hit rate of 31%, with a total of 170,725 hits as determined by Cheetah[59]. Diffraction patterns obtained from the hit finding step were fed into the CrystFEL software suite[60] (http://www.desy.de/~twhite/crystfel/) for indexing, integration and final merging from a total of 9,498 crystal diffraction patterns, with an estimated resolution cutoff beyond 4.6 Å, judged by the fall-off of crystallographic figures of merit, such as CC*.

Assignment of the space group $P3_1$ presented an indexing ambiguity, which was resolved using the "ambigator" software package within CrystFEL[61]. After running ambigator on the final data set, the indexing ambiguity did not appear to be perfectly resolved (judging by L-tests, etc.), most probably due to the number of diffraction patterns available for inclusion and the limited resolution of the diffraction patterns. The structure was determined by molecular replacement using PHASER[51] in the $P3_1$ space group with two PbgA monomers in the asymmetric with the PbgA full-length structure as a search model, which had all ligands and solvent removed. The TMD and periplasmic domain domains were refined as independent rigid bodies to allow for conformational flexibility within this different crystal lattice. Conservative refinement procedures were pursued and applying a merohedral twinning with operator [-k,-h,-l] in PHENIX REFINE[53] was ultimately found to return major improvements in map quality and R factors, compared to treatment of the data and refinement in the $P3_121$ space group with one PbgA monomer in the asymmetric unit, which yielded otherwise a similar crystal packing arrangement and overall electron density features. LPS was never refined in the $PbgA_{XFEL}$ structure due to the limited data resolution of this crystal form. All structural figures were generated using PyMOL[57] and all density maps were calculated to 4.6 Å, where the $F_o - F_c$ map was calculated before the inclusion of LPS to avoid introducing model bias from this ligand.

Molecular dynamics simulations

An all-atom model of PbgA in a lipid environment was generated from the high-resolution crystal structure using the Protein Preparation function in Maestro[62,63] which adds missing residues, side chains and hydrogens, predicts residue protonation states, and optimizes side chain conformations. LPS atoms without clear density were added using the builder function in Maestro. Two simulations were constructed as follows using the System Builder[63]. A LPS-PbgA simulation contained LPS, protein, lipids, water and ions, whereas a PbgA-only simulation did not contain LPS. In each case, the protein was placed in a 1-palmitoyl-2-oleoyl-*sn*-glycero-3-phosphoethanolamine (POPE) lipid bilayer. The bilayer was initially aligned manually to the region where the protein surface is most hydrophobic. The system was neutralized with the addition of five chlorine ions in the LPS–PbgA system and 11 chlorine ions in the PbgA-only (LPS removed) system. An orthorhombic box was constructed with a 15 Å buffer around the protein in all dimensions and the regions of the box not occupied by protein or lipid were filled with TIP3P waters. The resulting systems were then equilibrated using the relax_membrane.py[64] and Desmond multisim[65–67] programs.

Following equilibration, two production NPT simulations (LPS–PbgA and PbgA only) were run for 500 ns using Desmond, with a temperature of 300 K, pressure of 1.01325 bar and a 2 ps time-step. To assess whether the simulations had reached equilibrium, two new simulations were run with LPS swapped. Specifically, a second LPS–PbgA system was created using PbgA from the last frame of the 'PbgA only' simulation to which LPS was added. This second 'LPS–PbgA' system was re-equilibrated as described above and then run for an additional 500 ns of production simulation. Similarly, a second PbgA-only simulation was built using PbgA from the last frame of the first LPS–PbgA simulation, this time with LPS removed. The new PbgA-only system was re-equilibrated as described above and then run for 500 ns of production simulation. Protein movement was assessed by calculating the root mean squared deviation (r.m.s.d.) versus time using the Event Analysis tool in Maestro. For each of the four production simulations, the PbgA conformation from each time-step was first aligned to the crystal structure using Cα atoms, then the r.m.s.d. was calculated over all Cα atoms.

Multi-angle laser light scattering

Samples (100 µl) of purified PbgA proteins were injected onto a Waters XBridge BEH 200 column with a flow rate of 0.05 ml min^{-1}. The chromatography system was coupled to a three-angle light scattering detector (mini-DAWN TRISTAR) and a refractive index detector (Optilab DSP, Wyatt Technology). Data analysis was carried out using the ASTRA software. The experimental molar masses of *E. coli* and *S. typhimurium* PbgA (67.6 and 70.9 kDa respectively) were calculated with the protein conjugate analysis tool by subtracting the absorption and scattering contribution of dodecyl maltoside (dn/dc = 0.1435).

Differential scanning fluorimetry

Melting experiments were conducted on a Prometheus NT48 (NanoTemper technologies) by measuring the tryptophan fluorescence 330/350 nm ratio of protein samples concentrated at 0.5 mg ml^{-1} in a standard capillary. Standard deviations were calculated from three independent experiments performed with the same protein sample. Lipids (Avanti Polar Lipids) were mixed with purified PbgA protein at a final concentration of 0.1 mg ml^{-1} and incubated for 30 min at 4 °C before measurement.

Biolayer interferometry

Phospholipid (Avanti Polar Lipids) and Kdo_2-lipid A (US Biological Life Sciences) stock solutions were prepared by resuspension into 25 mM Tris pH 8, 100 mM NaCl, 0.05% LMNG buffer and solubilized overnight at 4 °C. Lipid stocks were diluted before experiments into 25 mM Tris pH 8, 100 mM NaCl, 0.5 mg ml^{-1} BSA, 0.05% LMNG. All assays were performed at 25 °C in 25 mM Tris pH 8, 100 mM NaCl, 0.5 mg ml^{-1} BSA, 0.05% LMNG. Biotinylated-LAB peptides were loaded onto SA biosensors to a response of approximately 0.5 nm. Binding to phospholipids and Kdo_2-lipid A was measured at concentrations of 150, 100, 50, 25 and 10 µM with 300 s association and dissociation steps. Assays were performed in triplicate on an Octet Red384 (ForteBio) and buffer and lipid signals were subtracted by using a biotin-blocked reference streptavidin (SA) biosensor. Dissociation constants for LAB_{WT} and LAB_{WT+} interactions with Kdo_2-lipidA were estimated by plotting response values at equilibrium as a function of concentration and fit to a global specific binding with Hill slope model in Prism (Graphpad Software).

Quantification of co-purifying LPS

The LPS content of purified PbgA, MsbA and Lnt proteins (25 ng ml^{-1}) was measured using a Limulus amebocyte lysate (LAL) chromogenic endotoxin quantification assay, according to the manufacturer's instructions (Pierce). A standard curve was generated using LPS from *E. coli* strain O111:B4, as directed by the manufacturer. All proteins were purified in LMNG detergent using matched conditions as described above. One endotoxin unit (EU) was assumed to equal 0.1 ng of LPS.

Extraction of Kdo_2-lipid A and detection by mass spectrometry

The extraction and detection of Kdo_2-lipid A was performed as previously described with minor modifications[68]. Four millilitres of hydrolysis buffer (50 mM sodium acetate hydrolysis buffer pH 4.5) was added to 50 µl of 40 mg ml^{-1} purified PbgA protein in a glass tube. The protein

suspension was sonicated for 5 min and then left in a boiling water bath for 30 min to cleave the O-antigen from Kdo_2-lipid A. After cooling to room temperature, lipid A was extracted by addition of 4.5 ml of chloroform (Arcos Organics) and 4.5 ml of methanol (Fisher Scientific). The solvents were vortexed thoroughly and separated by centrifugation at 1,000*g* for 10 min. The bottom organic layer was transferred to a new glass tube. Another 4.5 ml of chloroform was added to the remaining upper phase for the second extraction. After vortex and centrifugation, the bottom layers were combined and dried under a steady stream of N_2 gas. The resulting pellet was then dissolved into 10 µl of methanol–chloroform (1:4, v/v) for MALDI–TOF analysis. The 4800 plus MALDI–TOF/TOF Analyzer (AB Sciex) was equipped with a Nd:YAG laser using a 200 Hz firing rate. The matrix used was a saturated solution of 6-aza-2-thiothymine (Sigma-Aldrich) in 100% methanol. Samples were prepared by depositing 0.5 µl of matrix followed by 0.5 µl of the sample solution on the sample plate. After drying at room temperature, the spectra were acquired in the negative ion reflector mode.

Untargeted metabolomics

PbgA and MsbA samples were diluted to 100 µl reconstitution solvent to a concentration of 0.6 mg ml^{-1} (2:1:1 LC–MS grade water: methanol: acetonitrile) followed by ultra-sonication for 8 min in a room temperature water bath. Five microliters of each sample supernatant was injected for LC–MS analysis. Shimadzu series ultra-high performance liquid chromatography (UHPLC) system (Shimadzu) consisting of LC pumps (Model LC-30AD) with online degasser was used to deliver the mobile phases 5 mM ammonium acetate with 0.1% (v/v) formic acid in water (A) and 1 mM ammonium acetate with 0.1% (v/v) formic acid in acetonitrile:isopropyl alcohol (5:2, v/v) (B) at a flow rate of 0.3 ml min^{-1}. Samples (5 µl) were injected through an autosampler (ModelSIL30ACMP) with temperature control at 15 °C. Kinetex Evo C18 (100 × 2.1 mm 1.7µm; Phenomenex) reverse-phase column was used for liquid chromatography separation. Gradient liquid chromatography flow started with 5% B with a linear increase to 95% B in 30 min, followed by a 95% B hold for 5 min before returning to 5% B for column re-equilibration. The column oven (Model CTO30A) temperature was maintained at 40 °C.

Mass spectrometry analysis was performed on Orbitrap-Q Exactive HF-X instrument (Thermo Fisher Scientific) using Top 10 data-dependent MS^2 analysis based on intensity in both positive and negative modes (separate injections) with background ion exclusion lists. Ion exclusion list for positive and negative modes were created separately using buffer blank sample for dynamic software dependent exclusion of high intensity background ions (top 20 high intensity ions in the first half of LC runtime (0.5–20 min) and another top 20 in the second half (19.5–38 min). Data-dependent scan (dd-MS^2) settings for both positive and negative modes included a full MS scan from mass to charge ratio (*m/z*) of 113.5 to 1,700 at a resolution of 120,000 (full-width at half-maximum, FWHM), automatic gain control (AGC) target value of $1e^6$, maximum injection time (IT) of 200 ms and profile mode data acquisition. MS^2 settings included on the fly, top 10 high-intensity ions MS^2 fragmentation with a scan range of *m/z* 200-2000, resolution of 7,500 (FWHM), AGC target of 5×10^4, maximum IT of 10ms, isolation window of *m/z* 1.5 and profile mode data acquisition. Data-dependent settings included minimum AGC target of 5×10^2, intensity threshold of 5×10^4 with no multiple charge states and dynamic exclusion of 5 s. MS source parameters included Heated Electrospray Ionization (HESI) probe with spray voltage of 3.5 kV (positive mode) or 2.5 kV (negative mode), sheath gas flow rate: 49, auxiliary gas flow rate: 12, capillary temperature: 259 °C and funnel RF level at 80.0.

Data analysis to detect and identify unknown compounds with highest fold difference between PbgA (sample) and MsbA (control) was carried out in Compound Discoverer 2.1.0.401 metabolomics software (Thermo Fisher Scientific) using default workflow of 'Untargeted metabolomics with statistics and detect unknowns with mapped pathways (BioCyc beta) and ID using online databases (chem spider, mzcloud and KEGG)'. Data analysis also included protein purification buffer selected as blank in the analysis. Data processing workflow included default parameters for nodes such as input files, selecting spectra, aligning retention times, detecting and grouping unknown compounds, filling gaps, predicting compositions, searching mzcloud and chem spider databases, mapping to BioCyc (beta) and KEGG pathways, normalizing peak areas and marking background compounds. Sample to control MS peak area ratios and log_2-transformed fold changes were calculated in the data analysis and top identified compounds or molecular formula hits with peak area ratios higher than 5 (log_2-transformed fold change >2.6) are reported in Supplementary Table 4.

Generation of monoclonal antibodies against PbgA

Purified *E. coli* PbgA protein was reconstituted into liposomes for immunization by mixing it 1:1,500 molar ratio with *E. coli* polar lipid extract (Avanti Polar Lipids) overnight at 4 °C in the presence of biobeads for detergent removal. Large multilamellar vesicles were harvested by ultracentrifugation, resuspended in TBS and extruded through a 0.45-µm filter at room temperature. Mouse immunization and hybridoma generation were performed using standard protocols. Culture supernatants were assessed for high-affinity monoclonal antibodies using Octet (Fortebio) with anti-mouse IgG Fc capture biosensors for binding to purified PbgA proteins. Three clones were selected, scaled, and purified by standard methods for the co-immunoprecipitation experiments.

Co-immunoprecipitation and LC–MS/MS

Two milligrams of each antibody was applied to 100 µl MabSelect SuRe protein A resin (GE Healthcare) for 15 min in co-immunoprecipitation (co-IP) buffer (25 mM Tris pH 7.5, 150 mM NaCl, 0.025% LMNG). Unbound antibody was washed twice with 500 µl of co-IP buffer, and the beads were mixed with 50 ml of supernatant containing the matching overexpressed bait protein (according to conditions described in above method section) and incubated under gentle agitation for 2 h at 4 °C. Beads were collected by centrifugation at 2,000*g* for 4 min, then washed twice with 100 µl co-IP buffer, twice with 100 µl co-IP buffer supplemented with 350 mM NaCl, and once again with 100 µl co-IP buffer. Antibody–bait–prey complexes were eluted three times with 100 µl elution buffer (0.1 M glycine pH 3.5, 150 mM NaCl, 0.025% LMNG), and separated from beads and collected by centrifugation off a 0.2-µm filter into collecting tube preloaded with 100 µl 100 mM Tris pH 8 for quick neutralization of the acidic pH. Eluted proteins were separated by SDS–PAGE in Tris-glycine on a 4–20% polyacrylamide gel. Twenty bands per gel lane were excised, washed in 25 mM ammonium bicarbonate (Burdick and Jackson, 100 µl, 20 min), destained with 50% acetonitrile in water (100 µl, 20 min) and reduced with 10 mM dithiothreitol at 60 °C followed by alkylation with 50 mM iodoacetamide at room temperature. Proteins were digested with 0.2 µg trypsin (Promega) in ammonium bicarbonate pH 8 at 37 °C for 4 h. Digestion was quenched with formic acid and the supernatants were analysed directly without further processing by nano LC–MS/MS with a Waters NanoAcquity HPLC system (Waters Corp.) interfaced to a ThermoFisher Fusion Lumos. Peptides were loaded on a trapping column and eluted over a 75 µm analytical column at 350 nl min^{-1} (both columns were packed with Luna C18 resin from Phenomenex). A 30 min gradient was used (5 h total LC–MS/MS time per sample). The mass spectrometer was operated in data-dependent mode, with MS and MS/MS performed in the Orbitrap at 60,000 FWHM resolution and 15,000 FWHM resolution respectively. The instrument was run with a 3 s cycle for MS and MS/MS.

Proteomics analysis

Tandem mass spectrometric data were analysed using the Mascot search algorithm (Matrix Sciences) against a concatenated target-decoy database comprised of the UniProt *E. coli* K-12 protein sequences

(Taxonomy 83333, downloaded 1 July 2017), known contaminants and the reversed versions of each sequence. Peptide assignments were first filtered to a 1% FDR at the peptide level and subsequently to a 2% FDR at the protein level. Peptide spectral matches (PSMs) per protein were summed per sample across all fractions from the GelC-MS experiment. The Statistical Analysis of INTeractome (SAINT) algorithm (SAINTExpress-spc v.3.6.1)[69] was run with default settings comparing the sum of PSMs for all identified proteins enriched with each antibody separately (target) to the combined pool of control purifications (Supplementary Table 12). Interactions with a SAINT score >0.8 and Bayesian FDR < 0.05 were marked as significant.

Reporting summary

Further information on research design is available in the Nature Research Reporting Summary linked to this paper.

Data availability

Structural data are deposited in the Protein Data Bank (PDB) under accession number 6XLP. All mass spectrometry RAW files were uploaded to the MassIVE data repository, accessible by the identifier MSV000083754, and can be downloaded from ftp://MSV000083754@massive.ucsd.edu. DNA sequencing data were deposited at NCBI under BioProject PRJNA541088, BioSample SAMN11572257, experiment SRX5788703, run SRR9010525. The *E. coli* CFT073 reference genome was deposited at NCBI under BioProject PRJNA624646, BioSample SAMN14575425, accession CP051263. Source data are provided with this paper.

36. Datsenko, K. A. & Wanner, B. L. One-step inactivation of chromosomal genes in *Escherichia coli* K-12 using PCR products. *Proc. Natl Acad. Sci. USA* **97**, 6640–6645 (2000).
37. Chan, W. et al. A recombineering based approach for high-throughput conditional knockout targeting vector construction. *Nucleic Acids Res*. **35**, e64 (2007).
38. Lawrence, M. et al. Software for computing and annotating genomic ranges. *PLOS Comput. Biol*. **9**, e1003118 (2013).
39. Diederich, L., Rasmussen, L. J. & Messer, W. New cloning vectors for integration in the lambda attachment site attB of the *Escherichia coli* chromosome. *Plasmid* **28**, 14–24 (1992).
40. Baba, T. et al. Construction of *Escherichia coli* K-12 in-frame, single-gene knockout mutants: the Keio collection. *Mol. Syst. Biol*. **2**, 2006.0008 (2006).
41. Miller, J. H. *Experiments in Molecular Genetics* (Cold Spring Harbor Laboratory, 1972).
42. Mohammad, M. M., Howard, K. R. & Movileanu, L. Redesign of a plugged beta-barrel membrane protein. *J. Biol. Chem*. **286**, 8000–8013 (2011).
43. Kitagawa, M. et al. Complete set of ORF clones of *Escherichia coli* ASKA library (a complete set of *E. coli* K-12 ORF archive): unique resources for biological research. *DNA Res*. **12**, 291–299 (2005).
44. Alexander, M. K. et al. Disrupting Gram-negative bacterial outer membrane biosynthesis through inhibition of the lipopolysaccharide transporter MsbA. *Antimicrob. Agents Chemother*. **62**, e01142-18 (2018).
45. Karimova, G., Pidoux, J., Ullmann, A. & Ladant, D. A bacterial two-hybrid system based on a reconstituted signal transduction pathway. *Proc. Natl Acad. Sci. USA* **95**, 5752–5756 (1998).
46. Ladant, D. & Ullmann, A. *Bordatella pertussis* adenylate cyclase: a toxin with multiple talents. *Trends Microbiol*. **7**, 172–176 (1999).
47. Bligh, E. G. & Dyer, W. J. A rapid method of total lipid extraction and purification. *Can. J. Biochem. Physiol*. **37**, 911–917 (1959).
48. Caffrey, M. & Cherezov, V. Crystallizing membrane proteins using lipidic mesophases. *Nat. Protoc*. **4**, 706–731 (2009).
49. Otwinowski, Z. & Minor, W. Processing of X-ray diffraction data collected in oscillation mode. *Methods Enzymol*. **276**, 307–326 (1997).
50. Strong, M. et al. Toward the structural genomics of complexes: crystal structure of a PE/PPE protein complex from *Mycobacterium tuberculosis*. *Proc. Natl Acad. Sci. USA* **103**, 8060–8065 (2006).
51. McCoy, A. J. et al. Phaser crystallographic software. *J. Appl. Crystallogr*. **40**, 658–674 (2007).
52. Emsley, P., Lohkamp, B., Scott, W. G. & Cowtan, K. Features and development of Coot. *Acta Crystallogr. D* **66**, 486–501 (2010).
53. Adams, P. D. et al. PHENIX: a comprehensive Python-based system for macromolecular structure solution. *Acta Crystallogr. D* **66**, 213–221 (2010).
54. Winn, M. D., Isupov, M. N. & Murshudov, G. N. Use of TLS parameters to model anisotropic displacements in macromolecular refinement. *Acta Crystallogr. D* **57**, 122–133 (2001).
55. Ashkenazy, H. et al. ConSurf 2016: an improved methodology to estimate and visualize evolutionary conservation in macromolecules. *Nucleic Acids Res*. **44** (W1), W344–W350 (2016).
56. Holm, L. & Laakso, L. M. Dali server update. *Nucleic Acids Res*. **44** (W1), W351–W355 (2016).
57. The PyMOL Molecular Graphics System, version 2.0 Schrödinger, LLS.
58. Liu, W., Ishchenko, A. & Cherezov, V. Preparation of microcrystals in lipidic cubic phase for serial femtosecond crystallography. *Nat. Protoc*. **9**, 2123–2134 (2014).
59. Barty, A. et al. *Cheetah*: software for high-throughput reduction and analysis of serial femtosecond X-ray diffraction data. *J. Appl. Crystallogr*. **47**, 1118–1131 (2014).
60. White, T. A. et al. CrystFEL: a software suite for snapshot serial crystallography. *J. Appl. Cryst*. **45**, 335–341 (2012).
61. White, T. A. et al. Recent developments in *CrystFEL*. *J. Appl. Crystallogr*. **49**, 680–689 (2016).
62. Sastry, G. M., Adzhigirey, M., Day, T., Annabhimoju, R. & Sherman, W. Protein and ligand preparation: parameters, protocols, and influence on virtual screening enrichments. *J. Comput. Aided Mol. Des*. **27**, 221–234 (2013).
63. Schrödinger Release 2017-3: Schrödinger Suite 2017-3 Protein Preparation Wizard (New York, 2017).
64. Schrödinger Release 2017-3 (New York, 2017).
65. Shivakumar, D. et al. Prediction of absolute solvation free energies using molecular dynamics free energy perturbation and the OPLS force field. *J. Chem. Theory Comput*. **6**, 1509–1519 (2010).
66. Guo, Z. et al. Probing the α-helical structural stability of stapled p53 peptides: molecular dynamics simulations and analysis. *Chem. Biol. Drug Des*. **75**, 348–359 (2010).
67. Bowers, K. J. et al. Scalable algorithms for molecular dynamics simulations on commodity clusters. In *SC '06: Proc. 2006 ACM/IEEE Conference on Supercomputing*, 43–43) (Tampa, FL, 2006).
68. Hankins, J. V., Madsen, J. A., Needham, B. D., Brodbelt, J. S. & Trent, M. S. The outer membrane of Gram-negative bacteria: lipid A isolation and characterization. *Methods Mol. Biol*. **966**, 239–258 (2013).
69. Choi, H. et al. SAINT: probabilistic scoring of affinity purification-mass spectrometry data. *Nat. Methods* **8**, 70–73 (2011).
70. Berman, H. M. et al. The Protein Data Bank. *Nucleic Acids Res*. **28**, 235–242 (2000).
71. Ma, G., Zhu, Y., Yu, Z., Ahmad, A. & Zhang, H. High resolution crystal structure of the catalytic domain of MCR-1. *Sci. Rep*. **6**, 39540 (2016).
72. Mi, W. et al. Structural basis of MsbA-mediated lipopolysaccharide transport. *Nature* **549**, 233–237 (2017).
73. Noland, C. L. et al. Structural insights into lipoprotein N-acylation by *Escherichia coli* apolipoprotein N-acyltransferase. *Proc. Natl Acad. Sci. USA* **114**, E6044–E6053 (2017).
74. Vilar, S., Cozza, G. & Moro, S. Medicinal chemistry and the molecular operating environment (MOE): application of QSAR and molecular docking to drug discovery. *Curr. Top. Med. Chem*. **8**, 1555–1572 (2008).
75. Owens, T. W. et al. Structural basis of unidirectional export of lipopolysaccharide to the cell surface. *Nature* **567**, 550–553 (2019).
76. Ohto, U., Fukase, K., Miyake, K. & Shimizu, T. Structural basis of species-specific endotoxin sensing by innate immune receptor TLR4/MD-2. *Proc. Natl Acad. Sci. USA* **109**, 7421–7426 (2012).

Acknowledgements We thank our Genentech colleagues for their support, in particular, A. Song, I. Kekessie, J. Toms, E. Hecht, C. Peng, A. Liu, P. Smith, A. Estevez, C. Ciferri, H. Ho, E. Castellanos, A. K. Katakam, I. Zilberleyb, M. Reichelt, M.-W. Tan, J. Kiefer, Y. Franke, C. Koth, E. Brown and S. Hymowitz. We thank D. Cawley for antibody generation and Smartox Biotechnology for peptide synthesis. Use of the Linac Coherent Light Source (LCLS) and the Stanford Synchrotron Radiation Lightsource (SSRL), SLAC National Accelerator Laboratory, are supported by the U.S. Department of Energy, Office of Science, Office of Basic Energy Sciences under Contract No. DE-AC02-76SF00515. The SSRL Structural Molecular Biology Program is supported by the DOE Office of Biological and Environmental Research, and by the National Institutes of Health, National Institute of General Medical Sciences (P41GM103393). The contents of this publication are solely the responsibility of the authors and do not necessarily represent the official views of NIGMS or NIH. C.G. appreciates support from the SLAC National Accelerator Laboratory and Stanford University through a Panofsky Fellowship. All reagents are available under a materials transfer agreement with Genentech.

Author contributions T.C. and K.R.B. contributed equally to this work. T.C. purified and crystallized PbgA, with support from C.L.N. K.R.B., K.M.S., N.N.N., D. Swem and S.T.R. performed microbiology experiments. Q.L., P.L., E.V., G.H. and W.S. performed proteomics and lipidomics experiments, with support from T.C. J.R. and E.S. performed genomic sequence analyses. D. Sangaraju and S.S.-L. performed metabolomics experiments, with support from T.C. S.P. and M.X. performed in vivo experiments. L.M. and T.D.V. performed molecular biology and protein expression experiments. A.M. performed the LAL assay. D.P.D., M.S.H. and C.G. collected and processed SFX data. T.C. and J.P. determined and refined structures, with input from C.G. B.D.S. performed and analysed molecular dynamics simulations. J.P. proposed the lipid A-binding potential of PbgA-derived peptides and designed variants; N.S. and E.J.H. designed key peptides; M.R.-G. synthesized key peptides; T.C. performed lipid-binding interferometry experiments; K.R.B. and S.T.R. performed bacterial growth inhibition and MIC assays with peptides. T.C., K.R.B., S.T.R. and J.P. wrote the manuscript with input from all authors. J.P. and S.T.R. co-supervised the project and E.J.H., J.P. and S.T.R. are co-senior authors.

Competing interests All authors, except D.P.D., M.S.H. and C.G., are or were employees of Genentech/Roche.

Correspondence and requests for materials should be addressed to E.J.H., J.P. or S.T.R.

Peer review information *Nature* thanks Bert van den Berg, Russell Bishop, Changjiang Dong and the other, anonymous, reviewer(s) for their contribution to the peer review of this work.

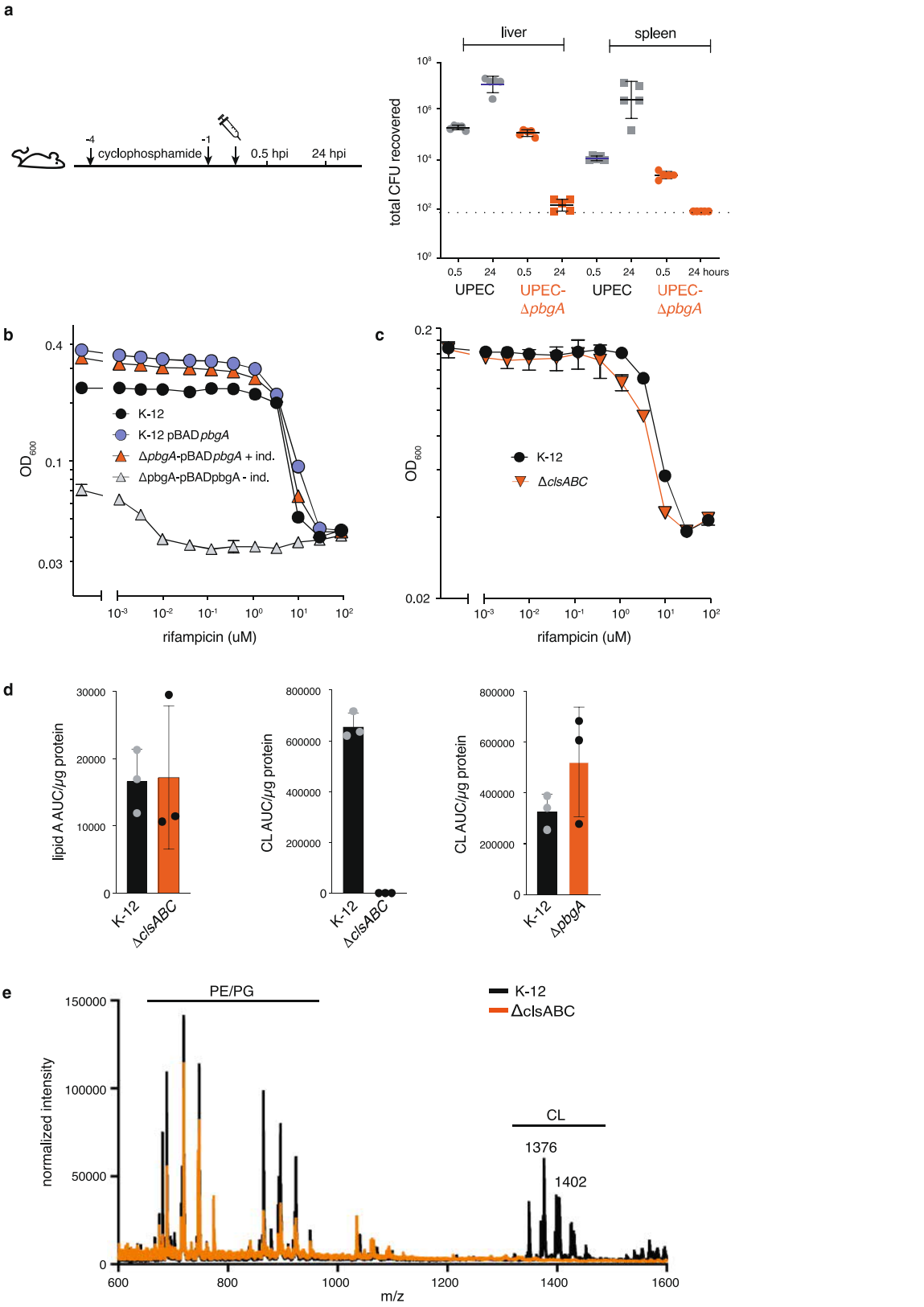

Extended Data Fig. 1 | In vivo and in vitro characterization of *E. coli* Δ*pbgA* and Δ*clsABC* strains. a, CFUs recovered from UPEC and UPEC Δ*pbgA* in neutropenic mouse tissues after intravenous injection of BALB/C mice 0.5 and 24 h after injection ($n = 5$ per group). Data are mean ± s.d. with dashed line indicating lower boundary of detection. **b**, Rifampicin sensitivity assay with conditional *E. coli K-12* Δ*pbgA::pBADpbgA* strain. Data are mean ± s.d. for at each rifampicin concentration for $n = 3$ of each strain. **c**, Rifampicin sensitivity assay with *E. coli* K-12 and Δ*clsABC* strains. Data are mean ± s.d. for each rifampicin concentration for $n = 3$ of each strain. **d**, Quantification of lipid A and cardiolipin measured by MALDI–TOF and Qtrap liquid chromatography–tandem mass spectrometry (LC–MS/MS), respectively, normalized to total protein amounts in whole cells (left and middle) or outer membrane vesicles (right). AUC, area under the curve. Data are mean ± s.d. for each strain for $n = 3$ replicates. **e**, MALDI–TOF mass spectrometry analyses detected no cardiolipin in the Δ*clsABC* strain (orange) compared to the *E. coli K-12* strain (black) when analysed under matched conditions. Representative results are shown.

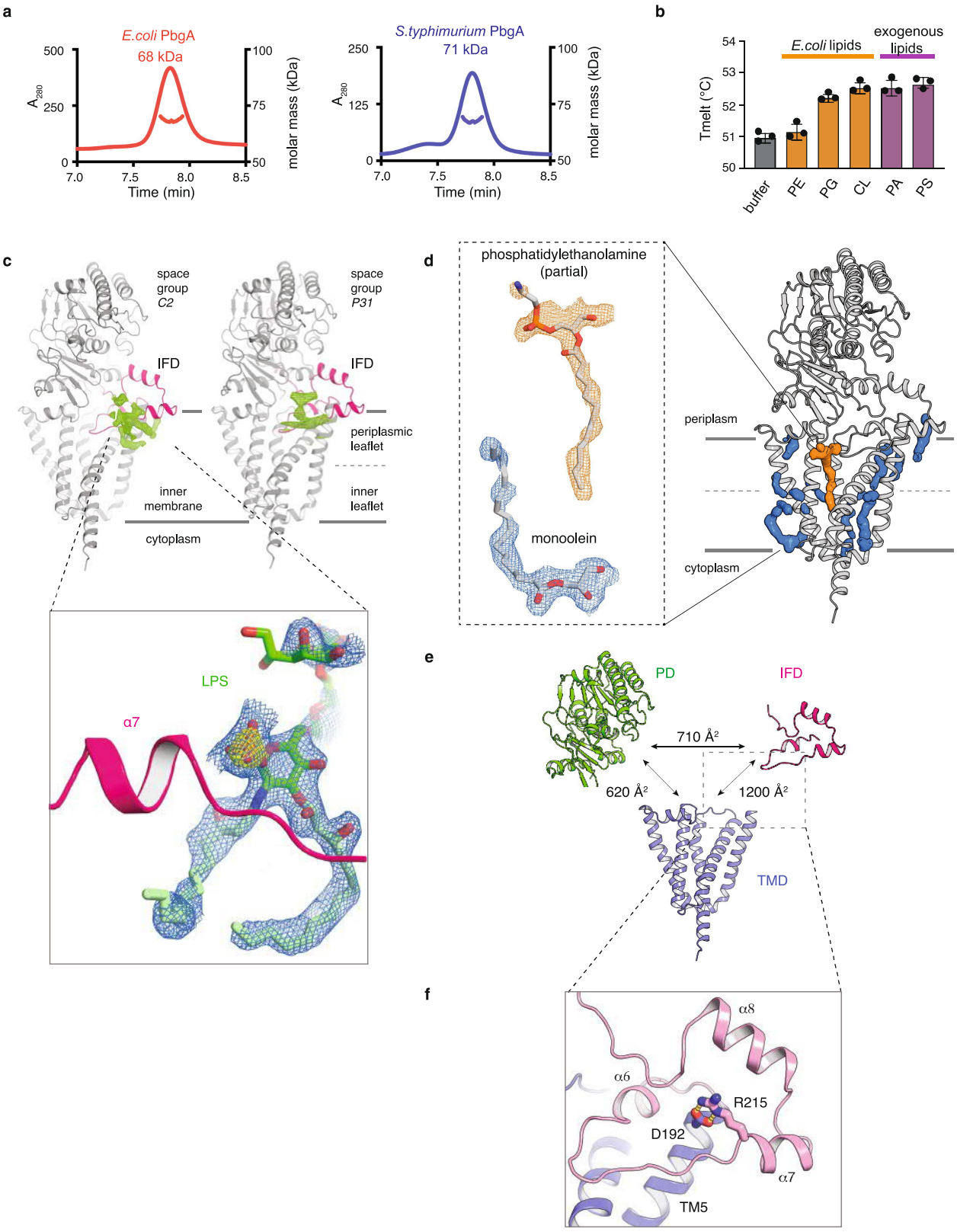

Extended Data Fig. 2 | See next page for caption.

Extended Data Fig. 2 | Biophysical and structural characterization of PbgA. **a**, *E. coli* and *S. typhimurium* PbgA were purified in the mild detergent dodecylmaltoside and analysed by SEC-MALS. **b**, Thermostability of purified *E. coli* PbgA was analysed by differential scanning calorimetry with or without 0.1 mg ml^{-1} lipid supplementation. **c**, Left, from PbgA crystalized in space group *C*2, using data to 2.0 Å, an $F_o - F_c$ map calculated shows bilobal extra electron density along the periplasmic membrane leaflet before the inclusion of LPS into models, 3σ contour. Inset, close-up view of an $F_o - F_c$ map calculated before the inclusion of LPS into the model, rendered at 8σ (yellow) and 2σ (blue), respectively. Final refined coordinates of lipid A are shown for reference. Right, from PbgA crystalized in space group $P3_1$, using data to 4.6 Å, an $F_o - F_c$ map calculated before the inclusion of LPS into the model, contoured at 3σ. **d**, Representative non-protein densities observed surrounding the TMD of PbgA that were assigned as putative phosphatidylethanolamine or monoolein lipids; inset shows $F_o - F_c$ maps calculated before the inclusion of phosphatidylethanolamine or monoolein into the model, 2σ contour (phosphatidylethanolamine, orange; monoolein, blue). **e**, Schematic illustration of the inter-domain surface area contacts within PbgA. **f**, Close-up view highlighting the interaction of the Arg215 side chain with a conserved acidic residue, Asp192 on TM5, which appears to stabilize the IFD–TMD interface.

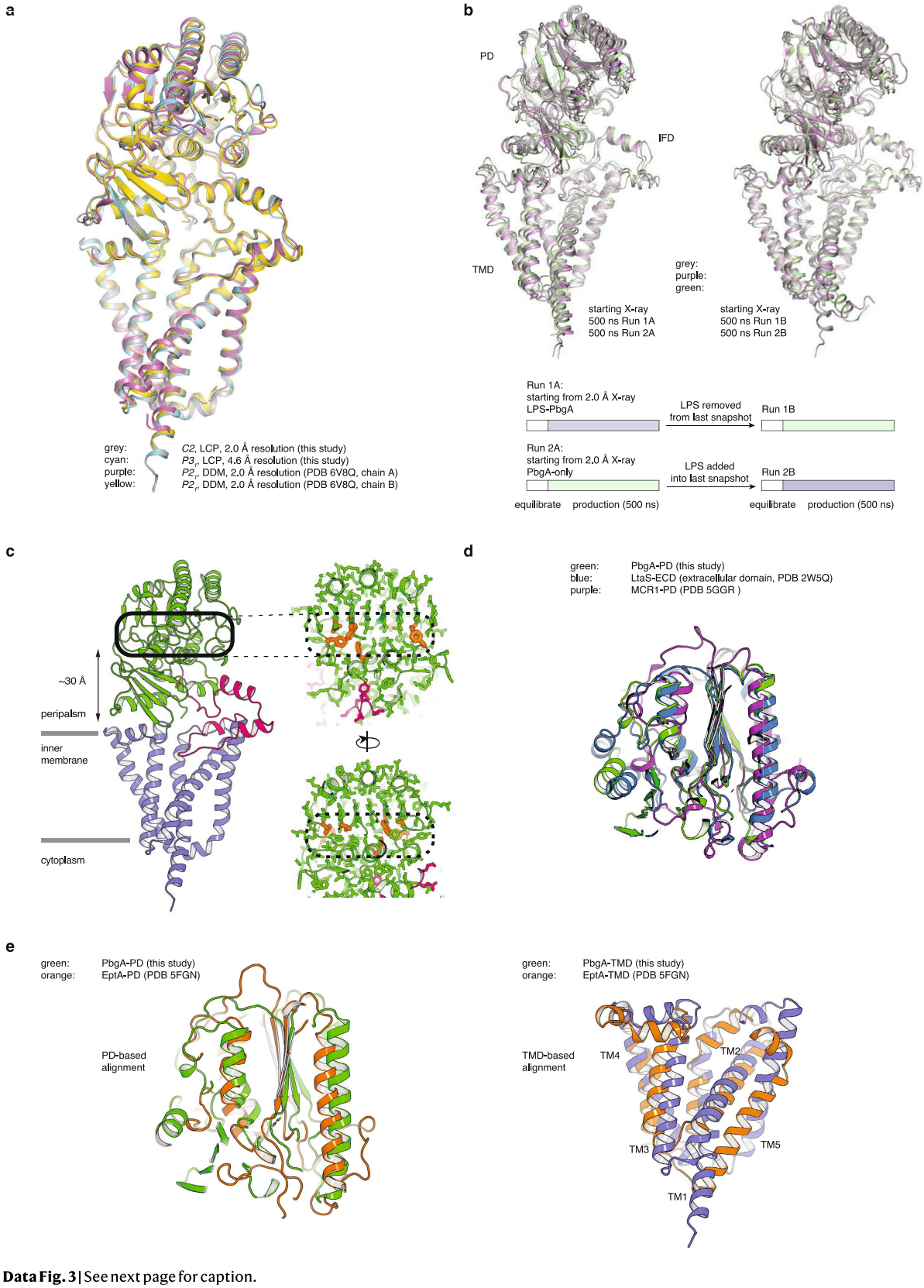

Extended Data Fig. 3 | See next page for caption.

Extended Data Fig. 3 | PbgA structural alignments and molecular dynamics simulations. a, Structural superposition of PbgA crystal structures determined in the present study (space group $C2$ and $P3_1$) and both chain A and chain B from PDB code 6V8Q. The overall root mean square deviation for main chain atoms between the most divergent structures is <0.8 Å. **b**, Molecular dynamics study of PbgA, results (top) and experiments (bottom) are summarized by illustration. Simulations were performed following preparation of the 2.0 Å PbgA crystal structure and its placement into a phosphatidylethanolamine: phosphatidylglycerol mixed membrane bilayer, as described in Methods. Top, superimposed are coordinates from the last frames of the four molecular dynamics simulation runs with the starting (non-relaxed) X-ray model to compare the extent of domain movements. **c**, Views of the previously proposed cardiolipin-binding site[8] are shown on the right. Residues proposed to be involved in cardiolipin binding are shown as orange sticks, but are seen here to form an integral part of the hydrophobic protein core; furthermore, the periplasmic domain of PbgA contains no recognizable sequence or structural homology to previously established lipid binding modules[56,70]. **d**, Structure-based alignment of the hydrolase superfamily domains from PbgA (periplasmic domain, green), *S. aureus* LtaS[22] (ECD, blue) and *E. coli* phosphoethanolamine transferase MCR-1[71] (periplasmic domain, purple). **e**, Structure-based alignment of PbgA and EptA isolated periplasmic domains (left) and TMDs (right), respectively.

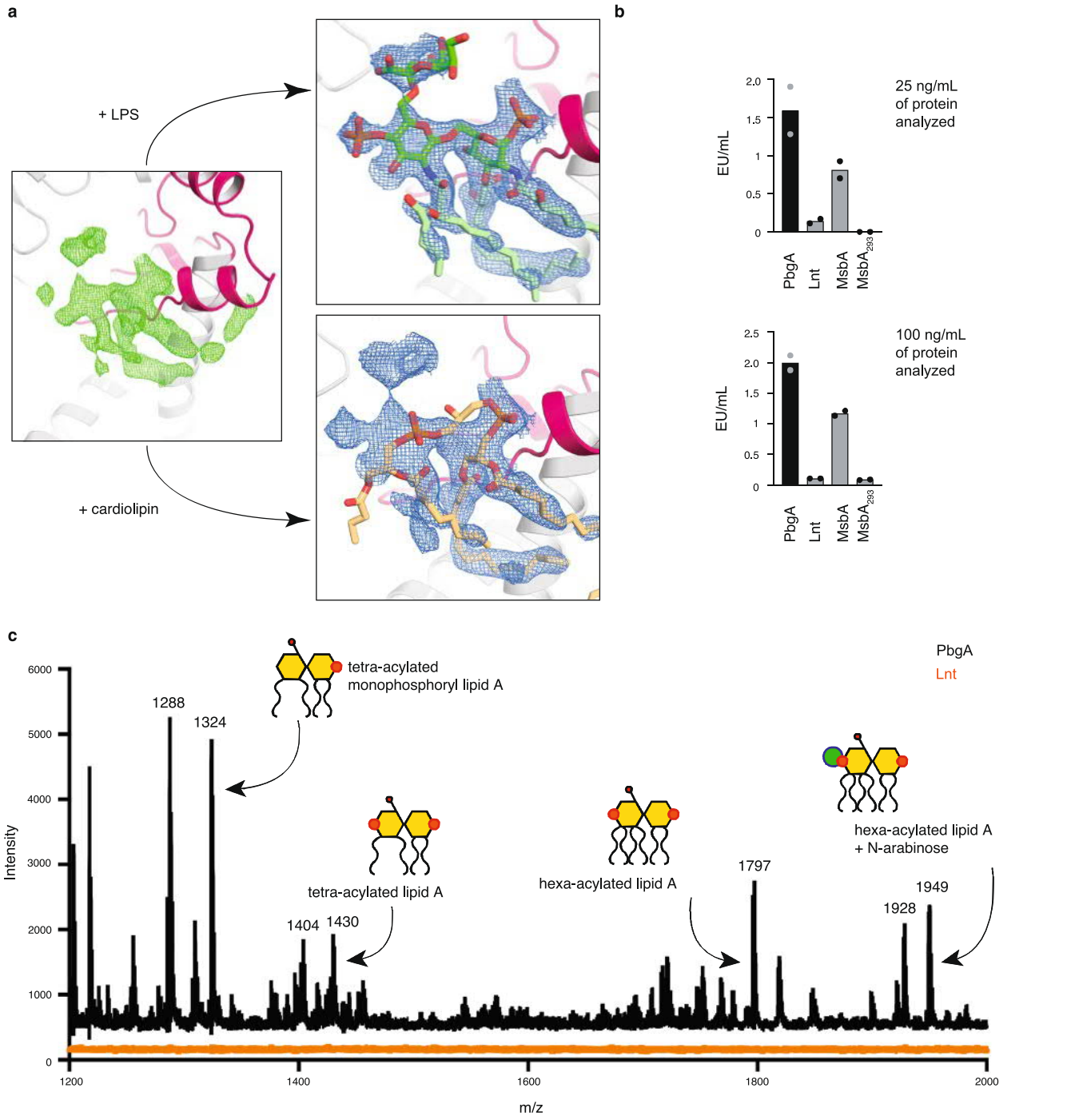

Extended Data Fig. 4 | LPS co-purifies and is bound to PbgA. a, Calculated using data to 2.0 Å, an $F_o - F_c$ map near the α7 helix of the IFD (pink) before inclusion of any ligand into refinement, 2σ contour (green). LPS refines well into this electron density whereas cardiolipin does not (see Extended Data Fig. 2c). Modelling and crystallographic refinement was pursued for cardiolipin, phosphatidylethanolamine, phosphatidylglycerol, monoolein and lauryl maltose neopentyl glycol (LMNG) detergent, but all efforts returned unacceptable refinement outcomes and maps. A $2F_o - F_c$ map following the inclusion of LPS into the refinement (blue, 0.8σ contour) is shown for reference. **b**, LPS quantification from proteins purified under matched conditions and subjected to a limulus amebocyte lysate assay. MsbA, the inner membrane LPS transporter from *E. coli*[29,72], was purified from a recombinant *E. coli* expression host and HEK293 cells ($MsbA_{293}$) for comparison. Lnt is an inner membrane protein involved that is not known or expected to bind or transport LPS[73], and was expressed and purified from *E. coli* for comparison. Experiments were run in duplicate at three different protein concentrations with similar results, where duplicate experiment with 25 ng ml^{-1} and 100 ng ml^{-1} protein are shown. **c**, MALDI–TOF mass spectrometry detects various lipid A species from purified PbgA, including an arabinose-modified species (black). No lipid A species were detected from Lnt purified and analysed under matched conditions (orange).

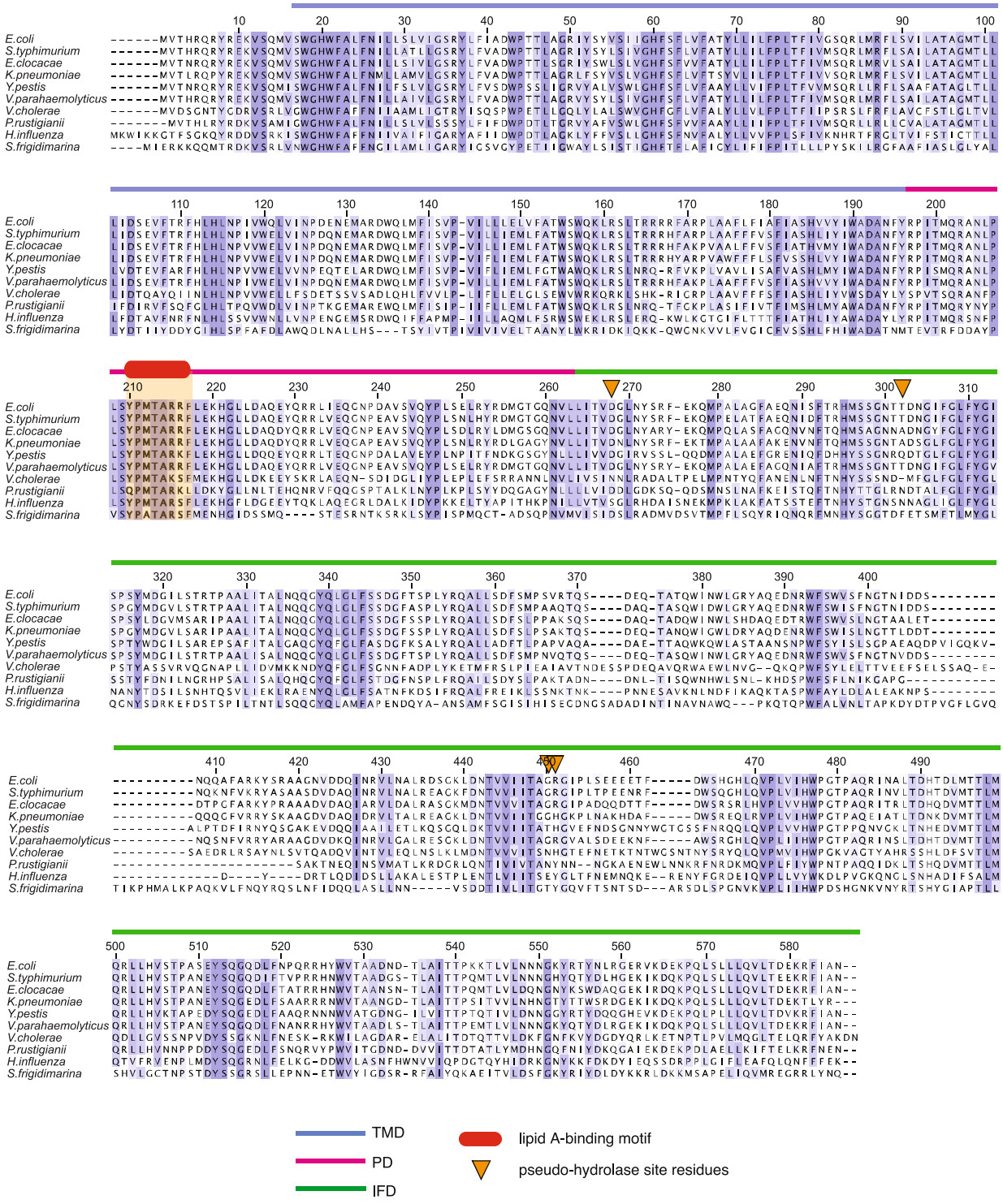

Extended Data Fig. 5 | Sequence alignment of then PbgA homologues. Sequence alignment of ten PbgA sequences from *Enterobacteriaceae* Gram-negative bacteria. Domain boundaries are based on *E. coli* PbgA structure are indicated, including the lipid A-binding motif (red shade) and pseudo-hydrolase active site residues (orange triangles).

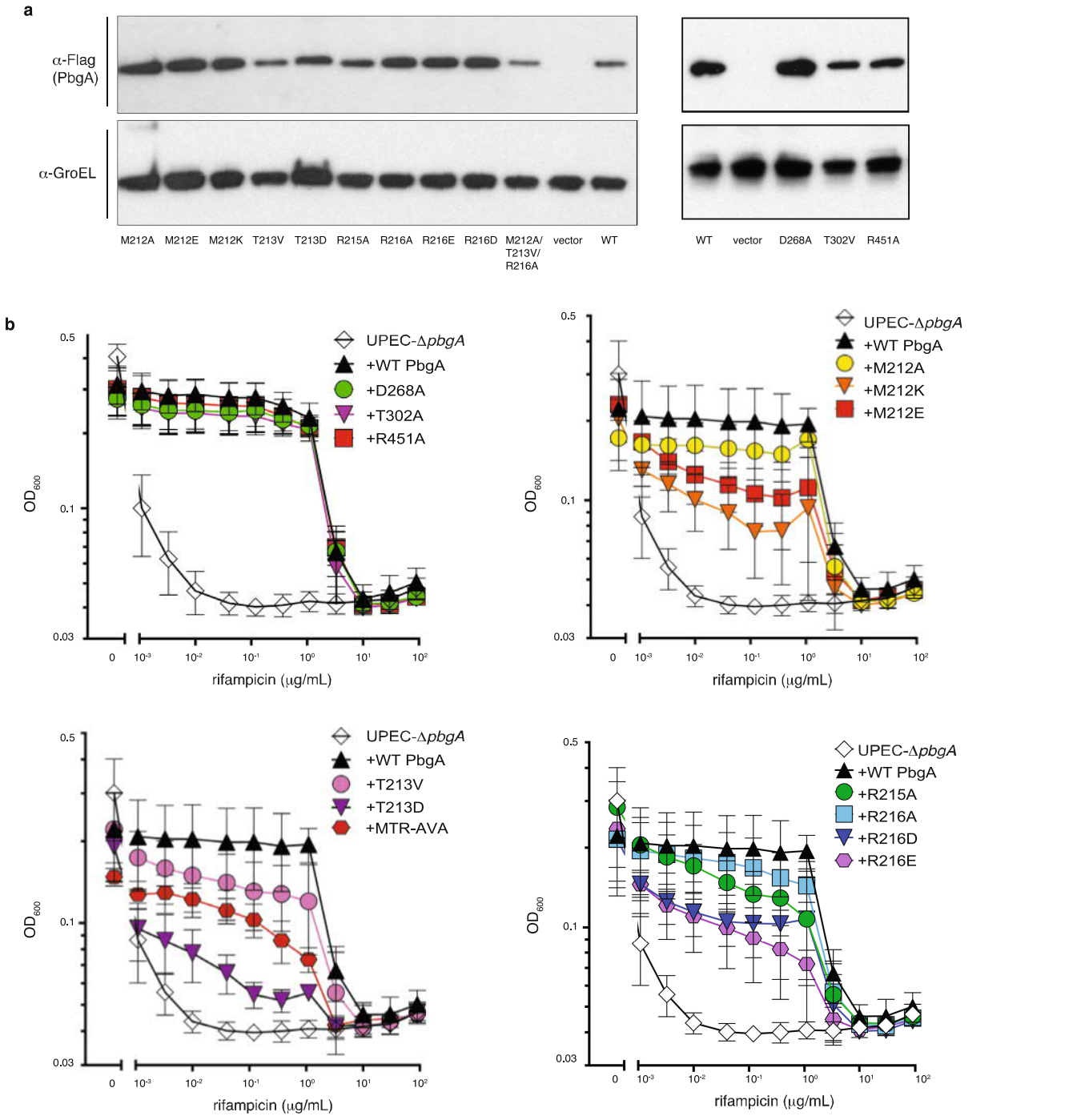

Extended Data Fig. 6 | PbgA mutants and outer membrane permeability. **a**, All UPEC-Δ*pbgA* bacteria tested in the rifampicin sensitivity assay were probed by western blot analysis to confirm PbgA–Flag expression. GroEL was assessed as a loading control. Representative blots for $n = 3$ or more experiments are shown. **b**, Outer membrane permeability of UPEC Δ*pbgA* strains with pBAD*pbgA* plasmids expressing wild-type or mutant *pbgA* assessed by rifampicin sensitivity, where MTR-AVA is the M212A/T213V/R216A PbgA triple mutant. Data are representative and presented as mean ± s.d. for $n = 3$ or more independent cultures. Note, see Extended Data Fig. 2f for a view of the salt-bridge interaction between R215 (IFD) and a conserved TMD acidic residue, D192.

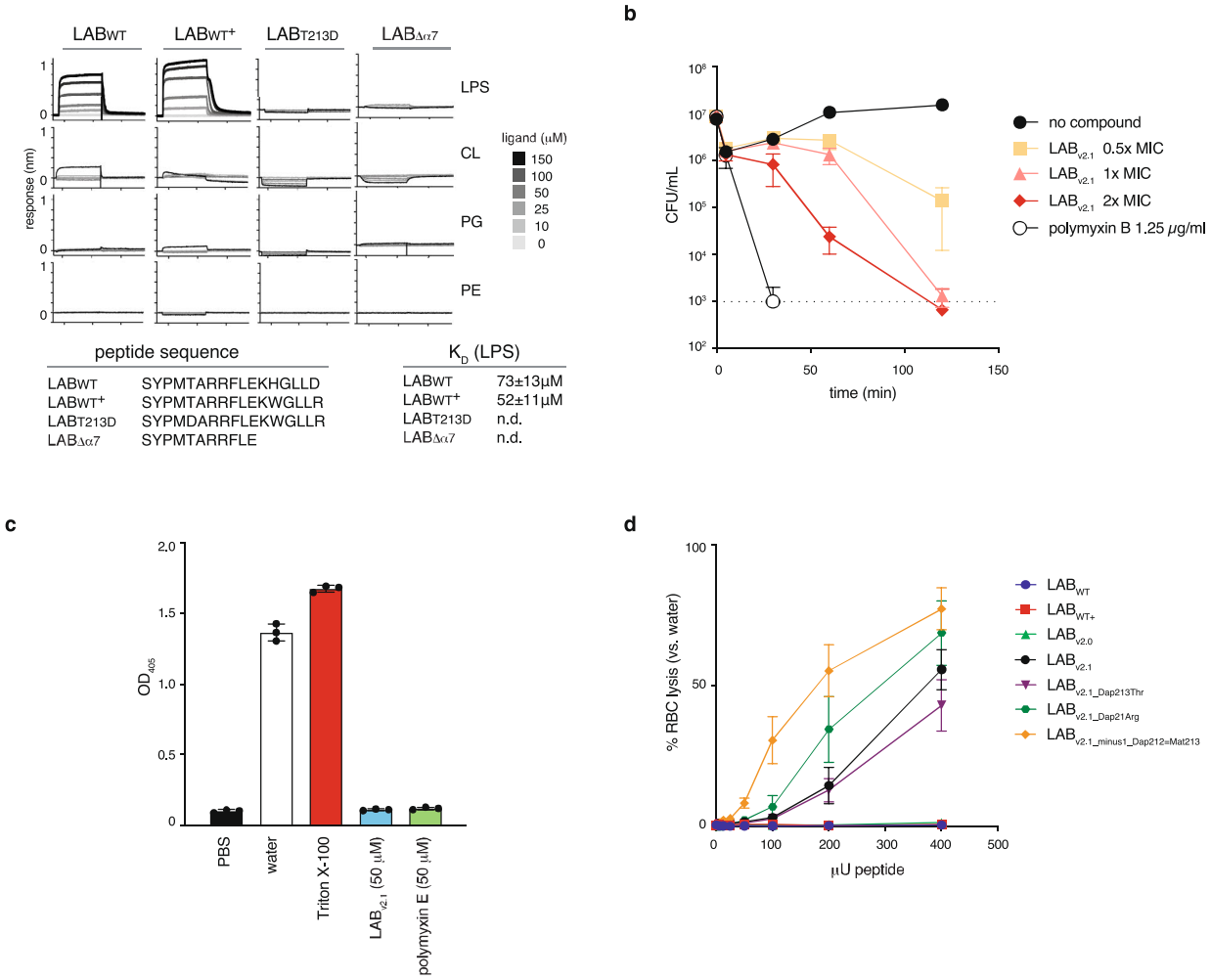

Extended Data Fig. 7 | Characterization of PbgA-derived, synthetic LAB peptides. a, Biotinylated LAB peptides were captured and interferometry measurements measured upon presenting peptides to different concentrations of detergent solubilized lipids (LPS, phosphatidylethanolamine, phosphatidylglycerol and cardiolipin). Three independent experiments were performed and data shown are representative. **b**, CFUs of *E. coli* ATCC 25922 measured over time with $LAB_{v2.1}$ and polymyxin B. Data are mean ± s.d. for $n = 3$ independent cultures. **c**, A red blood cell (RBC) lysis assay evaluated after 18 h in the presence of indicated compounds (Methods). Data are mean ± s.d. ($n = 3$) for each compound tested. **d**, A RBC lysis assay comparing $LAB_{v2.1}$ precursors (LAB_{WT}, LAB_{WT+}, $LAB_{v2.0}$) and $LAB_{v2.1}$ analogues designed, based on the LPS–PbgA crystal structure, to disrupt specific interactions of lipid A ($LAB_{v2.1\_Dap213Thr}$, $LAB_{v2.1\_Dap213Arg}$, $LAB_{v2.1\_Dap212\text{-}Met213}$). Data are mean ± s.d. for $n = 3$ independent assay of each compound at each concentration.

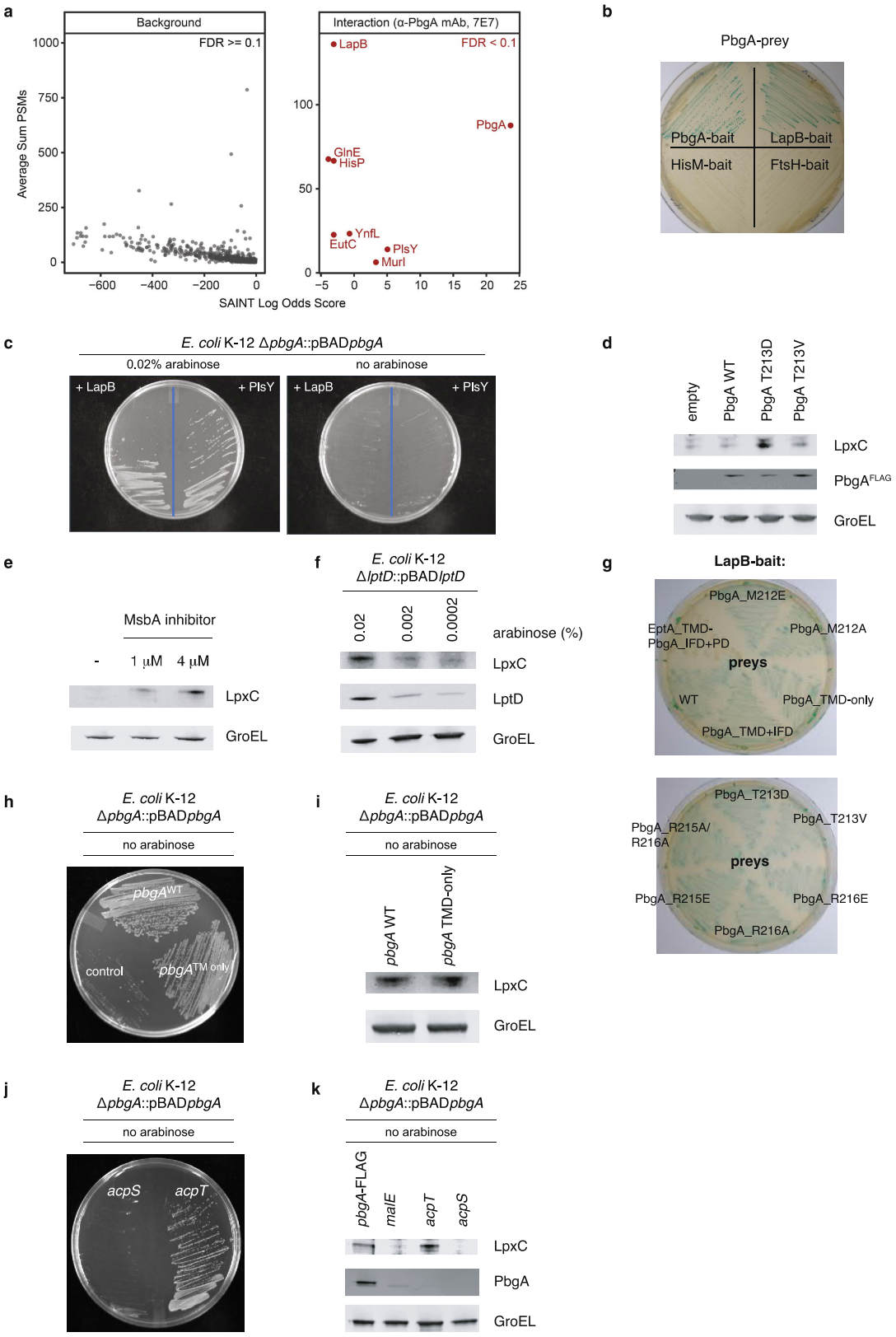

Extended Data Fig. 8 | See next page for caption.

Extended Data Fig. 8 | PbgA interacts with LapB to regulate LpxC stability. **a**, Proteins identified by mass spectrometry following co-immunoprecipitation of endogenous PbgA using the anti-PbgA monoclonal antibody 7E7 ($n = 3$ independent experiments). Hits were classified based on abundance (sum of PSMs) and enrichment in PbgA IPs compared to control purifications (SAINT logOddsScore: anti-PbgA monoclonal antibody 7E7 versus anti-gp120). Identified proteins with a Bayesian FDR <10% are highlighted in red. **b**, Bacterial two-hybrid system using PbgA-prey and different bait proteins in *E. coli* cells. Interacting proteins lead to blue colonies on agar plates containing X-gal, whereas non-interacting proteins produce white colonies. A representative agar plate is shown ($n = 3$) and activity was confirmed in broth cultures. **c**, Growth of a conditional *E. coli* K-12 Δ*pbgA*::pBAD-*pbgA* after depletion of PbgA in the presence of a IPTG-inducible plasmid expressing wild-type *lapB* or *plsY* (Methods) demonstrates that *lapB* expression does not rescue growth after PbgA depletion. Representative plates are shown and growth assay was repeated three or more times. **d**, Cell lysates prepared from overnight streaks of *E. coli* K-12 with pBAD*pbgA* wild-type or mutant plasmids were probed with anti-LpxC, anti-PbgA and anti-GroEL antibodies (Methods), indicating that disturbing the LPS–PbgA interaction interface leads to LpxC stabilization. Representative blots from $n = 3$ biological replicates are shown. **e**, Western blot analysis of LpxC after treatment with 1 μM (2× MIC) or 4 μM (8× MIC) of the small molecule MsbA inhibitor G'913, indicating that selective inhibition of MsbA[29,44] and LPS transport impacts LpxC levels; GroEL is the loading control and a representative experiment ($n = 3$ independent experiments) is shown. **f**, *E. coli* K-12 Δ*lptD*::pBAD*lptD* lysates prepared from cells grown in indicated concentration of arabinose were probed with anti-LpxC, anti-LptD and anti-GroEL antibodies (Methods). Representative blots from $n = 3$ biological replicates are shown. **g**, Bacterial two-hybrid assays using LapB-bait (pUT18-*lapB*) and indicated PbgA-mutant prey constructs (pKT25-*pbgA*) in *E. coli* DHM1 cells were performed (Methods). Interacting proteins lead to blue colonies, whereas non-interacting proteins produce white colonies. Note that $EptA^{TM}$–$PbgA^{IFD+PD}$ is a chimeric construct in which the TMD of PbgA has been replaced with the TMD region from EptA[23]. Representative plates from $n = 3$ culture streaks are shown. **h**, Growth of conditional PbgA strain (*E. coli* Δ*pbgA*::pBAD*pbgA*) in the absence of arabinose inducer complemented with, clockwise from the top of plate, wild-type *pbgA* ($PbgA^{WT}$), *pbgA* encoding only the TMD ($PbgA^{TM\ only}$), or a negative control (*malE*) on plasmids. A representative plate ($n = 3$) is shown. **i**. Cell lysates of the conditional *pbgA* strain (*E. coli* Δ*pbgA*::pBAD*pbgA*) in the absence of arabinose inducer complemented with wild-type *pbgA* or *pbgA* encoding only the TMD were probed with anti-LpxC antibody (Methods). A representative blot for $n = 3$ independent experiments is shown. **j**, Plasmids encoding *acpT* (right side of plate) or *acpS* (left side of plate) in conditional-*pbgA* strain grown in the absence of the pBAD*pbgA* inducer arabinose, with 0.1 mM IPTG at 30 °C. A representative growth plate ($n = 3$) was imaged. **k**, Cultures with plasmids expressing *pbgA*, *acpT*, *acpS*, *or malE* (control) were shifted to no arabinose/plus IPTG if necessary to deplete PbgA (Methods). A representative blot from at least $n = 3$ biological replicates is shown.

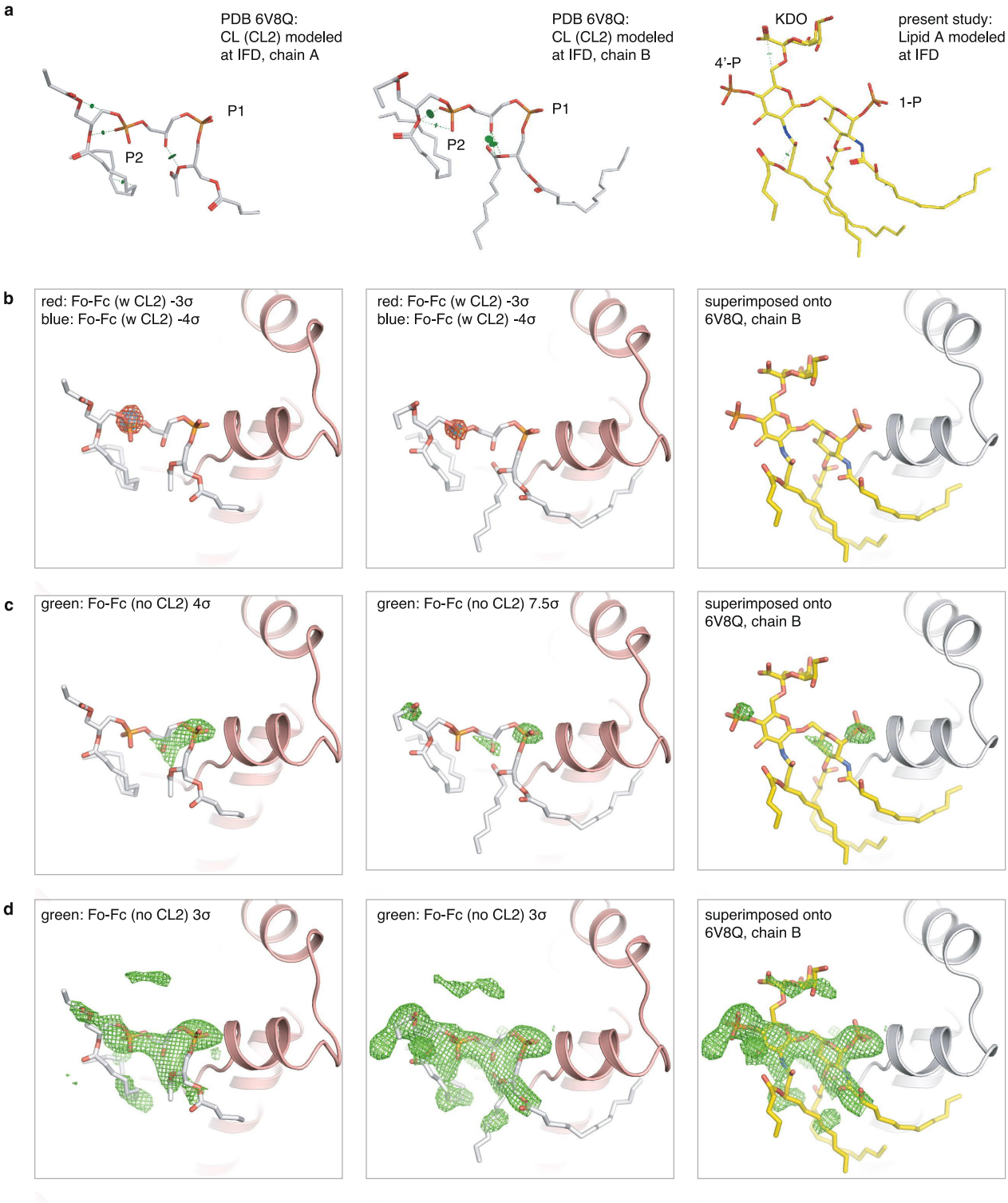

Extended Data Fig. 9 | See next page for caption.

Extended Data Fig. 9 | A previous PbgA crystal structure reported to have cardiolipin bound at the IFD is, instead, more consistent with bound lipid A. a, At the inner membrane–periplasmic interface that we term the IFD: cardiolipin (named CL2)[7] from chain A (left) and chain B (middle) of PDB 6V8Q are shown in stick representation; PbgA is removed for clarity. Similarly, lipid A is shown in stick representation taken from the high-resolution crystal structure presented in this work (right). Molecular clashes calculated using the MOE software[74] indicate high-energy atomic distance and poor geometry (green lines) in both chains A and B from PDB 6V8Q. The extent of the intramolecular clash is indicated by the relative size of the green circle. **b**, An $F_o - F_c$ map calculated using coordinates and structure factors from PDB 6V8Q chain A (left) and chain B (middle) shows a strong negative peak (-3σ, red mesh; -4σ, blue mesh) on the assigned modelled P2 phosphate position of the CL2 ligand. Right, the LPS–PbgA complex determined in this work is superimposed onto chain B of PDB 6V8Q for reference, with no further adjustments. **c**, An $F_o - F_c$ map calculated using coordinates and structure factors from PDB 6V8Q, with CL2 omitted from the calculation, shows strong positive peaks (4σ and 7.5σ for chain A and B, respectively; green mesh), which, in both cases, appear better described by the LPS–PbgA complex structure determined in this work. Shown (right) is the LPS–PbgA complex superimposed onto chain B of PDB 6V8Q with no further adjustments. **d**, The same $F_o - F_c$ map calculation as in **c**, only contoured to 3σ (green mesh). As seen on the right, when superimposed onto chain B of 6V8Q, the proximal 1-phospho-GlcNAc group of lipid A in our LPS–PbgA structure appears especially well accounted for by positive density peaks, and density consistent with a KDO sugar head group is also observed; and similar conclusions are reaching upon inspection of superposition onto chain A of 6V8Q (not shown).

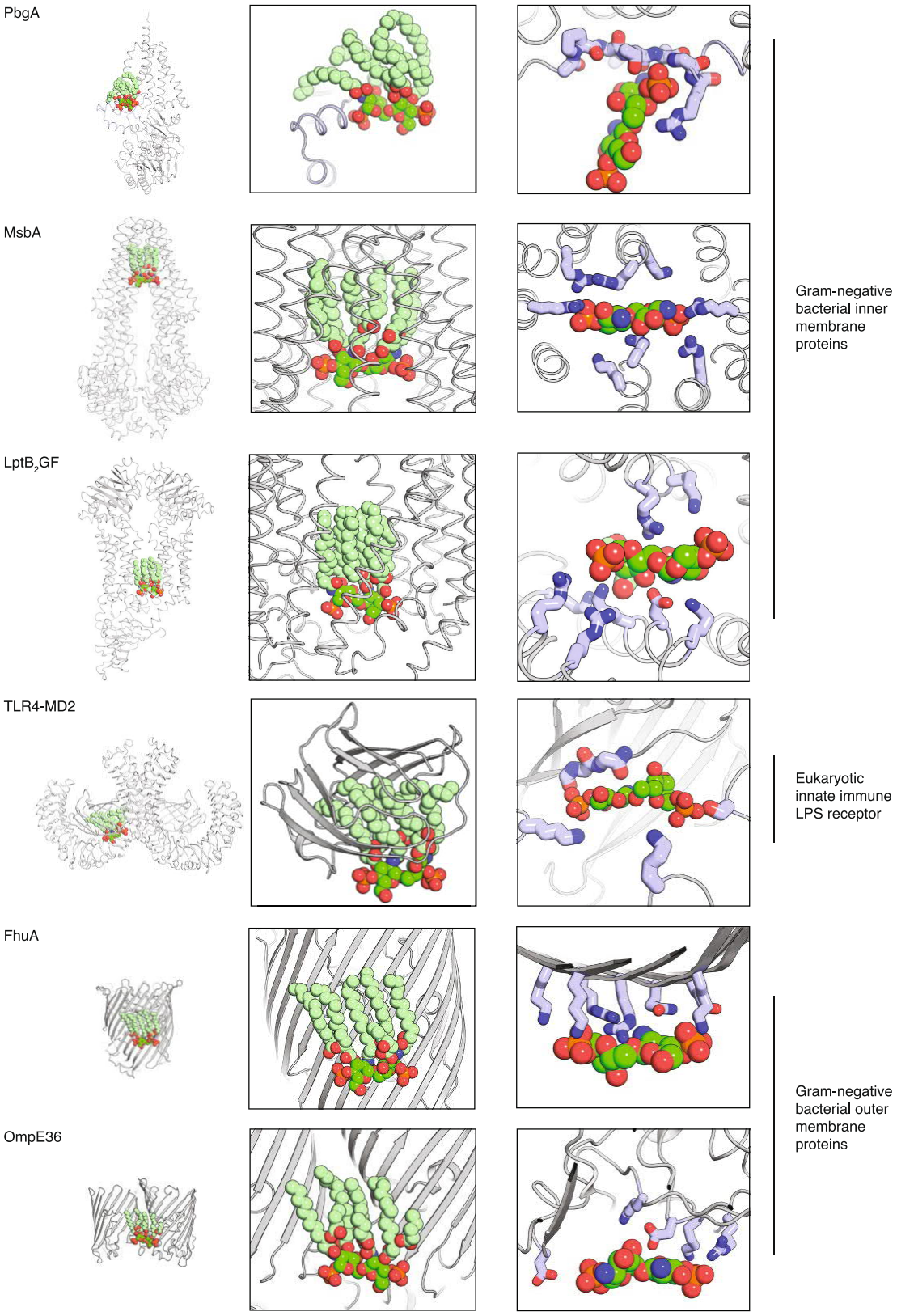

Extended Data Fig. 10 | See next page for caption.

Extended Data Fig. 10 | Comparison of LPS coordination in PbgA to known selective and passive LPS-binding proteins. PbgA (this study), MsbA (PDB code 6BPP), a selective LPS transporter[29,72], $LptB_2FG$ (PDB code 6MHU), a selective LPS[33,75], and TLR4-MD2 (PDB code 3VQ2), a high-affinity LPS receptor[32,76], represent the examples of selective LPS-binding proteins with known structures. In these latter cases, the hydrophobic acyl chains of lipid A are increased and the bivalent and polar nature are the lipid A head group is exploited. Furthermore, note that Arg216 of PbgA, shown in stick representation, does not appear essential for binding LPS in vivo (see Fig. 3c). In addition, FhuA (PDB code 2FCP), found with LPS complexed along the outer leaflet region of this outer membrane protein barrel[34], and OmpE36 (PDB code 5FVN), which has also revealed numerous LPS contacts along the barrel[35], are shown for completeness and comparison. Notably, analogous to MsbA, LptB2FG and TLR4, hydrophobic and aromatic side chains make several contacts in FhuA and OmpE36 with the acyl chains of lipid A (not shown for clarity) and polar and basic side chains coordinate the bivalent lipid A head group. In all cases, the lipid A coordination schemes are distinct from what is observed in the LPS–PbgA complex (also see Fig. 3).